MSc. Materials Science and Engineering

CAPE5000M Research Project

FINAL REPORT

Sintering and Reaction Behaviour of Electroless Nickel Plated Titanium and Copper Powders

Student: Mehmet Remzi Abul

Supervisor: Dr. Bob Cochrane

The University of Leeds

School of Chemical and Process Engineering

12 September 2017

ABSTRACT

Equimolar Ni-Ti and Ni-Cu powders pressed uniaxially using 500 MPa pressure and sintered for 1, 2, 4 and 8 hours. While Ni-Cu sintered at 900 ºC, sintering of Ni-Ti performed at 900 ºC and 1000 ºC in order to compare sintering behaviour at different temperatures. Electroless-nickel plating was used. Titanium and copper powders were electroless-nickel plated and sintered same as the non-plated powders in order to observe sintering behaviour difference. SEM and XRD were employed in order to investigate phases and microstructure of the samples. SEM and XRD data showed that electroless-nickel plated powders formed more intermetallics than non-plated powders.

ACKNOWLEDGEMENTS

I would like to thank my supervisor, Dr Bob Cochrane, for his support and guidance in my work. I would like to express my gratitude to him for his constant encouragement during my research.

Beside my supervisor, I would like to thank the university staff: Diane Cochrane, Robert Simpson, Stuart Micklethwaite and Faye Esad, who helped me during my experiments.

CONTENTS

ABSTRACT i
ACKNOWLEDGEMENTS ii
LIST OF FIGURES v
NOMENCLATURE vii
CHAPTER 1 1
INTRODUCTION 1
CHAPTER 2 3
LITERATURE REVIEW 3
2.1 Sintering 3
2.2 Sintering Stages 4
2.3 Effect of Sintering Variables 6
2.3.1 Green Density 7
2.3.2 Particle Size and Shape 7
2.3.3 Temperature 8
2.3.4 Sintering Atmosphere 9
2.4 Mechanisms of Sintering 9
2.5 Reactive Sintering 12
2.6 Nickel Titanium and Nickel Copper Phase Diagram 16
2.6.1 Nickel Titanium Phase Diagram 16
2.6.2 Nickel Copper Phase Diagram 18
2.7. Electroless Plating 19
2.8 Copper Nickel Alloys 21
2.9 Shape Memory Alloys 22
2.9.1 Shape Memory Effect and Superelasticity 23
2.9.2 Titanium-Nickel Shape Memory Alloys 24
CHAPTER 3 26
METHODOLOGY 26
3.1 Materials and Methods 26

3.1.1 Raw Materials 26
3.1.2 Preventing Pellets from Oxidation 27
3.1.3 Sintering 28
3.1.4 Sectioning of Samples 28
3.1.5 Grinding and Polishing 28
3.1.6 Etching 29
3.1.7 Electroless Nickel Plating 29
3.2 Characterization of Samples 30
3.2.1 Optical Microscope 30
3.2.2 Scanning Electron Microscope 31
3.2.3 Pore Fraction Calculation 31
3.2.4 X-Ray Diffraction 32
CHAPTER 4 33
RESULTS AND DISCUSSION 33
4.1 Results 33
4.1.1 Pore Fraction Change 33
4.1.2 Volume Change of Sinters 36
4.1.3 XRD Analysis 38
4.1.4 SEM Analysis 40
4.1.5 Electroless Nickel Plating 42
4.2 Discussion 45
CHAPTER 5 47
CONCLUSIONS AND FUTURE WORKS 47
5.1 Conclusions 47
5.2 Future Works 47
REFERENCES 48

LIST OF FIGURES

Figure 2.1: Two sphere sintering model which shows three stages of sintering [7]. 5
Figure 2.2: Schematic presentation of sintering mechanisms showing densifying and non-densifying mechanisms [4]. 10
Figure 2.3: Relation between phase diagrams and phase transformation during sintering in the contact region between heterogeneous particles [29]. 14
Figure 2.4: Nickel-Titanium binary phase diagram [33]. 17
Figure 2.5: Copper-Nickel binary phase diagram [36]. 18
Figure 2.6: Stress-strain-temperature data exhibiting the shape memory effect for a Ni-Ti SMA [58]. 24
Figure 3.1: Prevention samples from oxidation. 27
Figure 3.2: Electroless nickel plating, experimental set up. 30
Figure 3.3: SEM image (left) and binary image converted form SEM image by using ImageJ (right). 32
Figure 4.1: Binary Image of Cu-Ni sample sintered for 1 hr at 900 ^{o}C showing pores (in black) 34
Figure 4.2: Binary Image of Cu-Ni sample sintered for 1 hr at 900 C. Pores are shown in black. 34
Figure 4.3: Pore fraction change in Cu-Ni powder mixture. 35
Figure 4.4: Pore fraction change in Ni-Ti powder mixture. 36
Figure 4.5: Volume change of Cu-Ni powder mixture. 37
Figure 4.6: Volume change of Ni-Ti powder mixture. 38
Figure 4.7: XRD of sintered and polished Ti-Ni powder mixtures containing Ti, Ni, NiTi and $TiNi_3$ (sintered 4 hours at 900 ºC). 39
Figure 4.8: XRD of sintered and polished Ti-Ni powder mixtures containing Ti, Ni, NiTi and $TiNi_3$ (sintered 4 hours at 900 ºC). 39
Figure 4.9: SEM back scatter image (left) and elemental mapping (right) of the same sample sintered at 900 ºC for 4 hours showing elements (Ni in red, Ti in yellow). 41
Figure 4.10: SEM back scatter image (left) and elemental mapping (right) of the same sample sintered at 1000 ºC for 4 hours showing elements (Ni in red, Ti in yellow). 41

Figure 4.11: SEM backscatter image of Cu-Ni sintered at 900 ºC for 1 hour (left) and for 8 hours (right). 42
Figure 4.12: Electroless-nickel plated titanium powder with plating thickness of 3.71 micrometre. 43
Figure 4.13: XRD pattern of electroless-nickel plated and polished sample containing $TiNi_3$, TiO_2, NiTi and Ti (sintered at 900 ºC for 4 hours). 44
Figure 4.14: SEM backscatter image for nickel plated sample sintered at 1000 ºC for 4 hours showing intermetallic formed along the surface of titanium powder. 45

NOMENCLATURE

J…… Flux

D……...Diffusivity

C……Concentration

Γ……Rate Constant

k…….Boltzmann Constant

Ω……Solution Parameter

CHAPTER 1

INTRODUCTION

Sintering is a heat treatment process by which consolidated powders form a rigid body at elevated temperatures, usually at temperatures higher than half of the absolute melting point of the powders. Elevated temperatures increase the diffusional mass transport rate and promotes formation of new bonds between adjacent particles. Being one of the novel sintering techniques, reactive sintering offers production of oxides, carbides, borides and intermetallics. In reactive sintering, phase composition of the powder compact and the product is different.

Shape memory alloys are widely used in biomedical applications. Shape memory alloys recover their shape from deformed condition through heating. They gather this property because of the fact that the phase transformation between martensite and austenite is diffusionless and reversible. Production of these alloys via reactive sintering is an important issue for biocompatibility for some unique applications such as porous shape memory alloys. Ni-Ti alloys, specifically equiatomic NiTi intermetallic, are shape memory alloys used in biomedical application for their high biocompatibility. Thus, improvement in the production of these alloys are of interest for many scientists.

Copper has the excellent corrosion resistance properties in atmospheric and fresh water conditions. Nickel addition to copper gives a higher durability and strength as well as improving sea-water corrosion resistance. Excellent stress–corrosion cracking and

corrosion fatigue resistance makes Copper-Nickel alloys best choice for marine applications

In this project, reactive sintering behaviour of Ni-Ti and Ni-Cu system was investigated. While Ni-Ti forms intermetallics, Ni-Cu system is soluble for all composition. Electroless nickel plating is applied in order to increase intermetallics formed in Ni-Ti system. Effect of electroless nickel plating was investigated.

CHAPTER 2

LITERATURE REVIEW

2.1 Sintering

Sintering is a processing element in which powders pressed into desired shape is bonded together into a dense solid by applying external heat [1]. Sintering typically occurs at temperatures higher than half of the absolute melting point of powders. Having different morphologies like spheres, cubes, wires, flakes, and disks, powders used in sintering processes have diameter, usually less than 1mm. Small particles have relatively high surface area to volume ratio compared to large particles. These particles, during sintering process, reduce their surface energy by making new bonds and, consequently, removing free surfaces at elevated temperatures [2, 3].

Sintering is defined as “a thermally activated material transport in a powder mass or a porous compact, decreasing the specific surface by growth of particle contacts, shrinkage of pore volume and change of the pore geometry”. In other words, sintering is a heat treatment process, which results in the formation of new bonds between adjacent powders in order to decrease their surface free energies, which is known as driving force for

sintering. While one-component systems, homogeneous systems, can be sintered at temperature of 0.6-0.75 of absolute melting point of powders, multi-component systems, heterogeneous systems, require higher temperatures to be sintered [4].

Surface energy of the powders get larger when particle size gets smaller, which is due to high surface area volume ratio [5]. Thus, having higher driving force, smaller particles promote faster sintering and increase sinterability. Sintering reduces the surface energy by forming bonds between powders at the contact points, which consequently reduces free surfaces. In other words, powders form bonds and reduce free surfaces in order to have lower free surface energy, which is known as driving force for sintering. Powder size has also effect on the surface diffusion and the grain boundary diffusion, which are more likely favoured for the powders with smaller size. During reactive sintering of heterogeneous systems, liquid phase may form due to exothermic reaction of formation of intermetallic phases or formation of other phases such as borides, oxides and carbides. Liquid phase has higher mass transport rate than solid phase, which, as a result, improves sintering.

2.2 Sintering Stages

Sintering stages are described as the microstructural evolution of green compact into dense object. There are three stages of sintering process; initial stage, intermediate stage, and final stage [6]. Two sphere sintering model of these three stages is shown in Figure 2.1. Initial stage of sintering begins when the mobility of atoms is reached, and this stage ends when neck size exceeds one-third of particle diameter [7]. The formation of concave neck between adjacent powders, which provides strength and rigidity, starts in this stage. In this stage, even though neck formation is mostly predominated by volume diffusion, in the early stage, surface diffusion is the dominant transport mechanism since surface diffusion is initiated at relatively low temperatures when compared to volume diffusion, which requires higher temperatures to be initiated. Change in sintering parameters such as particle size, neck radius, green density, temperature and dwell time may chance the dominant mechanism [8].

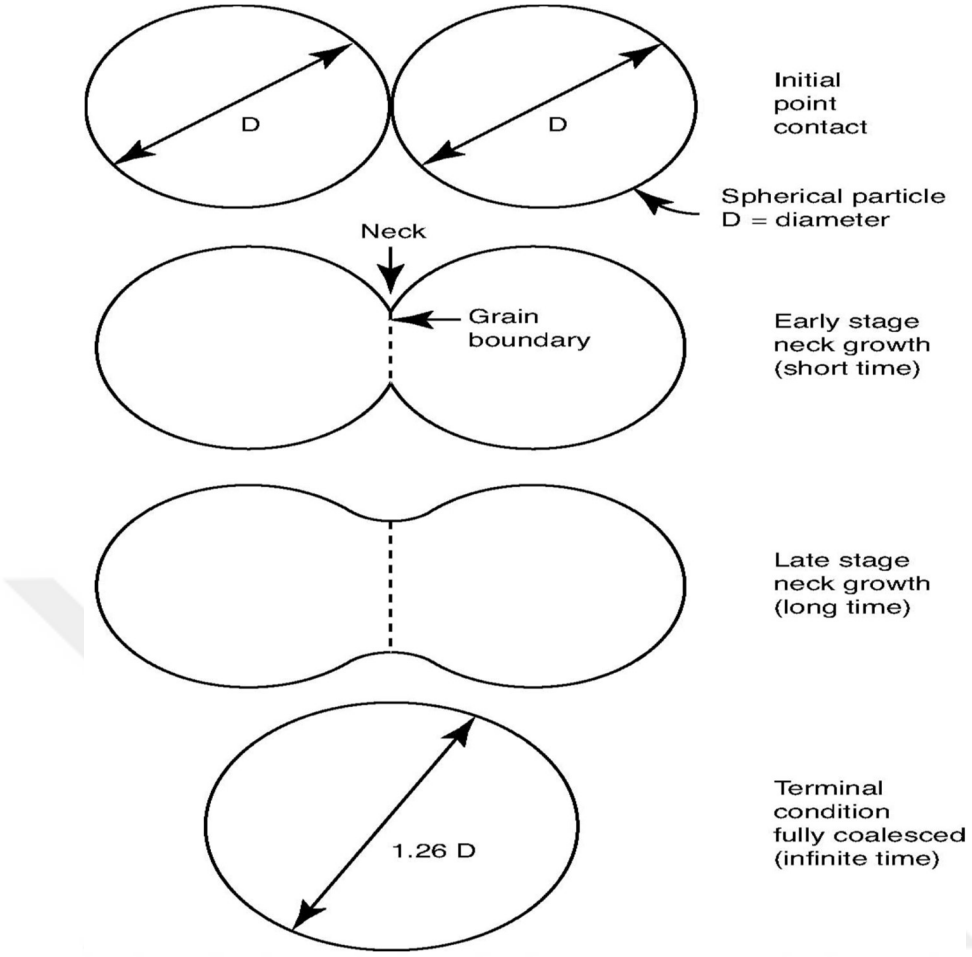

Figure 2.1: Two sphere sintering model which shows three stages of sintering [7].

The driving force for neck formation is energy gradient difference of different curvatures [9]. Neck formation of smaller particles is faster or starts at lower temperatures as smaller particles have higher surface free energy when compared to large particles. During initial stage of sintering, small amount of densification (decrease in porosity) occurs resulting in linear shrinkage which is around 3-5%. This linear shrinkage may correspond to around 70% of the theoretical density of the final sinter body [10].

Intermediate stage of sintering starts right after initial stage, when the neck size exceeds one-third of particle diameter. During this stage, solid particles form interpenetrating networks, which allow gaseous flow outside or inside of the sinter bodies [7]. Having lower neck curvature compared to initial stage, intermediate stage covers most of the densification, which can be up to 95% of the theoretical density of the final sinter. Grain boundary diffusion and volume diffusion are the dominant mechanisms in this stage. Pores

in this stage are interconnected and tubular, which allows gas to flow in or out [11]. At the end of this stage grain growth starts and connection between pores are closed due to neck growth and creation of new contact points, which may result in entrapment of gaseous in the sinter bodies [5]. Low green density may cause grain size coarsening without densification. This stage ends when neck size to particle size ratio is 0.5.

Isolation of channel-like pores, when neck size to particle size ratio exceeds 0.5, is the start of the final stage of sintering. Ideally, remaining porosity is expected to be eliminated and maximum density may be achieved at the end of this stage. However, extensive grain growth may take place during the elimination of last few percent of pores. Thus, conventionally powders are sintered until the final density being around 99.5% of theoretical density. Otherwise, extensive grain growth would take place and result in decrease in the mechanical properties of final product [12].

At the last stage of sintering Ostwald Ripening, also referred as Lifshitz-Slyozov-Wagner (LSW) theory, coarsening of precipitates, pores and particles, can be observed. According to Ostwald Ripening theory if size of a particle is smaller than critical radius, particle will dissolve [13]. If it is bigger than critical size, it will grow bigger. That is to say that while pores having size bigger than critical radius will grow and inhibit the densification, pores smaller than critical size will be dissolved and perished.

2.3 Effect of Sintering Variables

Sintering variables directly affect the sinterability and final microstructure of final sinter bodies and as a result these variable influence mechanical properties and other properties of sinter body [14]. Sintering variables can be divided into two sub sets: material variables and process variables [15]. Material variables are composition of powder compact, powder size, green density, powder shape. Process variables are temperature, sintering atmosphere, dwell time, heating rate and cooling rate. Process variables consist of thermodynamic variables and kinetic variables.

2.3.1 Green Density

Green density is defined as the density of the powder compact. Sintered density, final density of sinter, directly depends on the green density of the powder compact so that powder compacts with green density below 45% of the theoretical density are hard to sinter to desired or theoretical density due to insufficient contact surface between adjacent powders [16]. Shrinkage for low density compacts comparably high because of the fact that green compacts with lower density has higher pore volume to be shrunk in order to reach final density, which makes the dimensional control of the final sinter bodies impossible [17]. This high shrinkage in final sinter bodies also causes higher sintering stress during elimination of pores and results in relatively high change in the density as well as dimensions. Thus, dimensional control of low density compacts are hard to set and if sintering stress is so high, cracks may form inside the sinter body.

Higher green density, not less than 60% of theoretical density, provides more contact interface (plane where two different phases meet and interact, and where reaction take place during sintering) and, as a result, increases the densification process and rate. Dimensional difference of green compact and sinters is not as high as in the case of low density green compact. High green density also decreases and retards excessive grain growth during final stage of sintering [18].

2.3.2 Particle Size and Shape

Particle size accelerates sintering by increasing the mass transport rate [19]. In other words, the smaller the particle size is, the shorter sintering times can be achieved. Small particles can be sintered at relatively lower temperatures compared to large particles due to improvement in sintering rate. Sintering rate is improved because of the fact that small particles have higher interfacial energy than large particles. Small particle size also improves the densification rate [20]. Densification rate is indirectly proportional to the particle size so that densification rate can be given as $1/G^m$, where G is the particle size and m represents diffusion mechanism. The value of m depends on the dominant diffusion

mechanism taking place during sintering so that m=4 for grain boundary diffusion and m=3 for lattice diffusion.

On the other hand, green density of small particles, especially nanoscale particles, which have particle size less than 100 nm in diameter, is very low due to packing problems [21]. In addition, since small particles have higher free surfaces, oxidation becomes a really important issue during production of powders. Powders have very thin oxide layer on the surface which gets dissolved during early sintering process. Since small particles have higher free surfaces, the amount of oxides on the surface of small particles is very high when compared to coarse particles. Consequently, dissolved oxygen can form pores during cooling of sinter bodies and limit final density of sinter.

Not only particle size but also particle shape affects the sintering process. Particle shape directly changes green density and, as a result, densification rate and diffusion rate [7]. Having the highest green density due to random packing, spherical particles enhance the densification rate. However, spherical particles have less surface area to volume ratio compared to nonspherical particles such as acicular, irregular rod like, flake and dendritic particles. Considering surface energy as the driving force for sintering, nonspherical particles are expected to sinter faster than spherical powders. Nevertheless, nonspherical particles are lack of green density and contact interface.

2.3.3 Temperature

Sintering is a thermally activated process. All the diffusion mechanisms are dependent on temperature and they are risen exponentially with the rising temperature. Thus, higher sintering temperatures provide shorter sintering time by increasing diffusion rate. In most cases, logarithm of sintering time is inversely proportional with temperature. Temperature may also change compounds formed during sintering. For example, as the Ni-Ti phase diagram suggests (Figure 2.4), during sintering of titanium and nickel powders if the sintering temperature is higher than 984 ºC, where peritectic reaction take place: L + NiTi➔ Ti_2Ni, formation of Ti_2Ni is not observed since above this temperature this intermetallic is not thermodynamically stable. Temperature also changes the activation energy of elemental particles when particles undergo phase transformation. Alpha titanium, for instance, transforms into beta titanium at 862 ºC and activation energy for

self-diffusion increases from 192 kJ mol^{-1} to 328 kJ mol^{-1}. Nickel addition decreases activation energy to 142 kJ mol^{-1}. While Ni, Fe and Co have high diffusivity in both alpha and beta titanium, other metals have different diffusivity in different phases of titanium [22].

2.3.4 Sintering Atmosphere

There are several functions of sintering atmosphere. Sintering atmosphere is mainly applied to avoid or to control chemical reactions. These reactions can be oxidation, reduction, carburisation, decarburisation etc. Among these prevention from oxidation is the most important one. Except noble metals and advanced oxide ceramics, sintering should be performed under oxygen free atmosphere; vacuum or protective atmosphere such as argon and helium. Formation of oxide on the surface of the powder may retard or stop the diffusion and, consequently, efficiency of sintering process. For example during sintering of aluminium, which forms a very stable oxide on the surface, if oxygen is present in the system, alumina is formed on the surface of the powders and this oxide inhibits the diffusion of aluminium and other substances and, consequently, stops the sintering process. Similarly, chromium forms a very stable oxide and this oxide stops further diffusion of other substances. On the other hand, titanium has different mechanism of oxidation. Titanium powders are also covered with very thin (10 nm) oxide layer like other metallic powders [22]. However, unlike in the case of aluminium and chromium, this oxide layer (Rutile, TiO_2) dissociates and dissolves around 550 ^oC in the alpha titanium.

2.4 Mechanisms of Sintering

During sintering process, when liquid phase is not present, several mass transport mechanisms take place [4]. These mechanisms can be divided in to 2 subsets; densifying mechanisms, cause shrinkage and, as a result, increasing the density of sinter bodies, and non-densifying mechanisms, which does not change the final density of the final product. Schematic presentation of sintering mechanisms are given in Figure 2.2. Effect of

densifying mechanisms increases with increasing temperatures. On the other hand, non-densifying mechanisms are more likely active at lower temperatures.

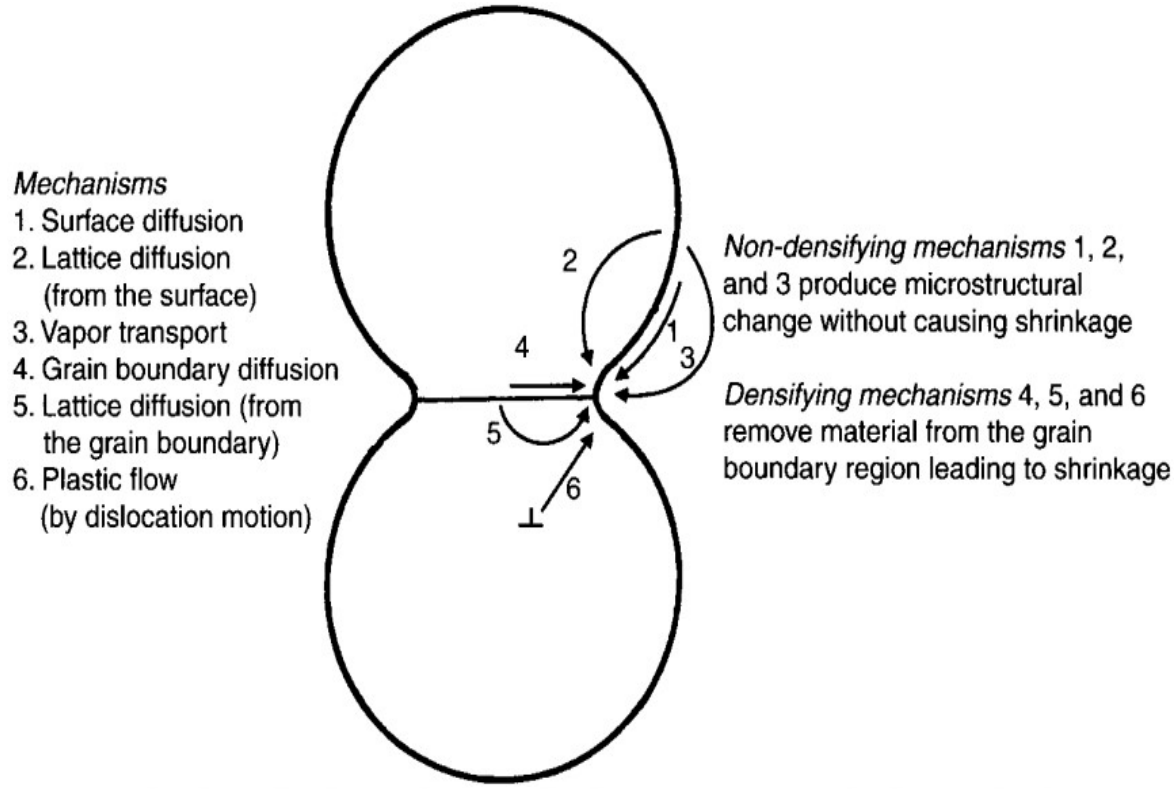

Figure 2.2: Schematic presentation of sintering mechanisms showing densifying and non-densifying mechanisms [4].

Surface transport processes are the non-densifying mechanisms. Non-densifying mechanisms include vapour transport, surface diffusion, and lattice diffusion (from the surface) [23]. These mechanisms do not change the density of the sinter bodies. Their contribution is to speed up neck growth and they also coarsen the particles. Sintering temperature determines the dominant process so that vapour transport is only active at relatively high temperatures, while others active for all temperatures [24]. Surface transport is only active at high temperatures since it requires the highest energy to proceed. Surface diffusion, which is known as the initial contributor for all sintering processes, is caused by the defects present on the rough surface of powders. Since surface diffusion requires the lowest activation energy, it becomes active and the dominant mechanism at lower temperatures. Even though surface diffusion is not the leading mechanism for sintering process, when it comes to powders with small particle size, especially nano sized powders, surface diffusion becomes the dominant mechanism. That is because of the fact

that small particles have very high surface free energy. Elevated temperature and slower heating rates promote the surface diffusion. However, this is not desired for most cases because surface diffusion does not make any contribution to densification process. Thus, higher heating rates produces denser sinters by lowering surface diffusion rate [4].

Grain boundary diffusion, lattice diffusion (from the grain boundary) and plastic flow are the densifying mechanisms [23]. These bulk transport mechanisms provide densification as well as contributing neck growth and coarsening of the particles by vacancy motion in crystal structure. During heating of green compact, plastic flow is the leading mechanism of bulk diffusion since plastic flow is dependent on the dislocation density, which increases when the temperature of the system increases. Plastic flow is more likely to be observed when small particles used and high heating rates applied. However, grain boundary diffusion and volume diffusion contribute the densification mechanism more than plastic flow during sintering. Small grains, having more grain boundary surface, cause to promote grain boundary diffusion [24].

Grain boundary diffusion is the most important mechanism for densification of sinter bodies. Activation energy needed for grain boundary diffusion is higher than surface diffusion but lower than that needed for volume diffusion [4]. Although energy needed is relatively low, grain boundary diffusion is directly dependant on the number of grain boundaries, in other words grain size of the sinter bodies. Grain boundary diffusion is more likely favourable in materials with low grain size which provide more surface area for diffusion. High grain boundary energy may result in excessive grain growth at the final stage of the sintering process. Addition of grain boundary segregate formers reduces the effect by lowering grain boundary energy [23].

Motion of vacancies in crystal matter is called as volume diffusion or lattice diffusion. Although factors affecting volume diffusion are temperature, composition and pressure, when it comes to compounds dominant factor is stoichiometry. In other words, compounds formed during sintering may change the sinterability of the powders. Since stoichiometric compounds have higher vacancy concentration than non-stoichiometric compounds, stoichiometric compounds accelerate the sintering process. Non-stoichiometric compounds formed at the interface slow down the diffusion rate because bonding forces in non-stoichiometric compounds are bigger than bonding forces in stoichiometric compounds.

Bonding forces in non-stoichiometric compounds are sometimes so big that they can even stop the diffusion of species. Contribution of volume diffusion in sintering can be expressed by Fick`s first law of diffusion,

$$J = -Dv\frac{dC}{dx} \qquad \text{(Equation 2.1)}$$

where J is the flux of vacancies, D_v is diffusivity or diffusion coefficient, dC/dx is vacancy concentration change in unit distance. Temperature and composition of sinter are very important because diffusivity and vacancy concentration vary with temperature.

Fick's first law is valid under steady state condition. On the other hand, Fick's second law of diffusion predicts the concentration change with time under unsteady state condition. Fick's second law of diffusion is given as

$$\frac{\partial C}{\partial t} = -\frac{\partial J}{\partial x} = D(\frac{\partial^2 C}{\partial x^2}) \qquad \text{(Equation 2.2)}$$

Where C is depletion or accumulation of concentration, J is the flux of the atoms (number of atoms per unit are in unit time).

2.5 Reactive Sintering

During sintering of heterogeneous particles, reaction may take place and, as a result, new constituents such as borides, carbides, oxides, nitrides, intermetallics, etc. would form. Formation of these constituents is exothermic which means that once the reaction initiated, heat released is large enough to self-sustain the sintering process without need of any external heat input [26]. Kinetic model of diffusion controlled reactions can be given as [27]

$$1\text{-}(1\text{-}\beta)^{1/3} = \Gamma t^{1/2} \qquad \text{(Equation 2.3)}$$

Where β is the fraction transformed, Γ is the rate constant and t is isothermal time. Γ is temperature dependant variable of the equation which can be given as [27]

$$\Gamma = \Gamma_0 \exp\left(-\frac{Q}{kT}\right) \qquad \text{(Equation 2.4)}$$

Where Q is activation energy, k is Boltzmann`s constant, T is absolute temperature, and Γ_0 is the frequency factor.

Self-sustaining reactions are also called as self-propagating high-temperature synthesis (SHS), gasless combustion, thermal explosions, or reactive sintering. In reactive sintering elemental powders are used to form compounds (Equation 2.5) [4].

$$xA + yB \rightarrow A_xB_y \qquad \text{(Equation 2.5)}$$

Reactive sintering is a sintering process through which new phases are formed. In other words, phase composition of green compact and final product are different. During reactive sintering densification occurs together with combustion synthesis [27, 28]. Reactions between constituents in reactive sintering release heat which increases the temperature of the system. Due to exothermic nature of these reactions, a liquid phase, which helps densification by increasing diffusion rate, may form. Being an endothermic process, melting lowers the maximum temperature of the system. Particle size of powders used is an important parameter during reactive sintering, as well as green density, since reactions take place at the contact points.

During sintering of two different metal powders not only diffusion mechanisms but also alloy phases, such as intermetallics and solid solution, formed and these compounds effect the growth rate and densification process [7]. Compounds formed during sintering may affect the rate of diffusion, especially volume diffusion. Depending on the compound formed during neck formation, in the initial stage of sintering process, growth rate of neck can be enhanced, retarded or may not change. Formation of neck for three different systems: complete solid solution, small solid solubility and intermetallics are given in Figure 2.3. Figure 2.3 also represents phases formed. Alloy formation reactions take place as soon as neck forms where two particles are in contact with each other.

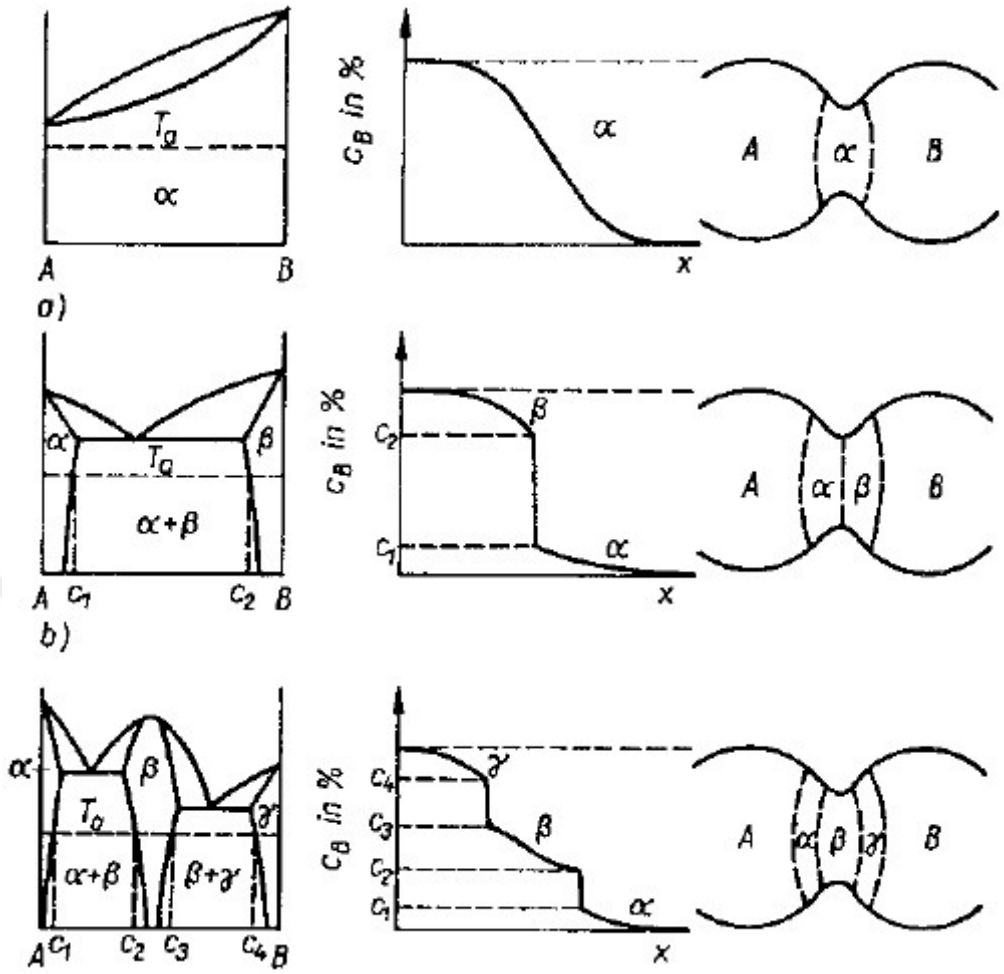

Figure 2.3: Relation between phase diagrams and phase transformation during sintering in the contact region between heterogeneous particles [29].

Unlike solid phase sintering in which the driving force is reduction in surface energy, the driving force for reactive sintering is chemical reactions between particles [29]. That is because driving force for chemical reactions are much higher than the decrease in surface energy, driving force for solid state sintering. New phases formed during reactive sintering may result in swelling (increase in volume) instead of shrinkage due to the change in specific volume of new compounds and depending on the density of the new constituents formed. Another reason of swelling is the inequality of diffusivities on the movement of particles, which is known as Kirkendall Effect [4]. In other words, Kirkendall Effect occurs when diffusivity differences of species are comparably different. For example, diffusion coefficient of nickel in titanium is faster than diffusivity of titanium in nickel, which means that nickel moves faster in titanium than titanium in nickel. This difference in diffusivities results in the formation of pores in the microstructure of final product.

Another example is copper-nickel system. Copper has larger diffusion coefficient in nickel. In addition to Kirkendall Effect, atomic mobility of elements slows down in intermetallics formed during reactive sintering due to strong bonding forces in intermetallics. Formation of liquid phase, due to exothermic nature of reactions, overcomes swelling and increases the densification of sinter body.

Reactive sintering is also used for production of metal-ceramic and ceramic-ceramic composites. For example, TiC-Al_2O_3-Al metal-ceramic composite is produced by reactive sintering and the formation reaction is given as [4]

$$3TiO_2 + (4+y)\,Al + 3C + Al_2O_3 \rightarrow 3\,TiC + (2 + x)\,Al_2O_3 + y\,Al \qquad \text{(Equation 2.6)}$$

Chemically active systems, which forms new phases, have much higher free energy of mixing than surface energy. This difference can be as high as hundreds of times [30]. The free energy of mixing, ΔG_{mix}, is given in Equation 2.7 [31].

$$\Delta G_{mix} = \Delta H_{mix} - T\Delta S_{mix} \qquad \text{(Equation 2.7)}$$

where T is the temperature, ΔS_{mix} is entropy of mixing and ΔH_{mix} is enthalpy of mixing.

Enthalpy of mixing is given as [31]:

$$\Delta H_{mix} = \Omega\, x_A x_B \qquad \text{(Equation 2.8)}$$

Where x_A and x_B are fractions of A and B, respectively, and Ω is solution parameter, which represents combinations of energy of bonds generated and broken between atoms A and B. Combinations are A-A, B-B, A-B and B-A [31]. Thus, Ω can be given as [31]:

$$\Omega = \varepsilon_{AA} + \varepsilon_{BB} - 2\varepsilon_{AB} \qquad \text{(Equation 2.9)}$$

Thermodynamically, heat of mixing must be negative for a reaction to be favoured. Thus new bonds formed between species must have high bonding energy. Negative heat of mixing also means that reaction taking place is exothermic.

2.6 Nickel Titanium and Nickel Copper Phase Diagram

Phase diagrams are very important to make a link between microstructure and properties of any materials, especially alloy systems. Alloy phase diagrams help to understand change in alloy properties during heat treatment and to improve these properties. Since sintering is defined as a kind of heat treatment process [4], understanding of phase diagrams becomes a really important issue.

2.6.1 Nickel Titanium Phase Diagram

In the Nickel-Titanium phase diagram (Figure 2.4), there present a number of phase transformations. These phase transformations are very important for heat treatment, improvement of shape memory alloys as well as sintering of shape memory alloys. Important phase transformations in this binary system are eutectic at 942 ^{o}C (Equation 2.10), eutectoid at 765 ^{o}C (Equation 2.11), and peritectic at 984 ^{o}C (Equation 2.9).

$L \rightarrow \beta Ti + Ti_2Ni$ (Equation 2.12)

$\beta Ti \rightarrow \alpha Ti + Ti_2Ni$ (Equation 2.13)

$L + TiNi \rightarrow Ti_2Ni$ (Equation 2.14)

There are three intermetallics present in Nickel-Titanium system which are Ti_2Ni, TiNi and $TiNi_3$. While other intermetallics are stoichiometric, TiNi phase is nonstoichiometric. During sintering of NiTi, formation of other phases is unavoidable that is due to the fact that Ti_2Ni and $TiNi_3$ are thermodynamically more stable than TiNi. Apart from these intermetallics Titanium-Nickel system forms other intermetallics such as Ni_3Ti and Ni_4Ti_3 during production from elemental powders. These intermetallics are thermodynamically metastable and lead formation of stable phase of $TiNi_3$ as shown in Equation 2.15 [32].

$Ti_3Ni_4 \rightarrow Ti_2Ni_3 \rightarrow TiNi_3$ (Equation 2.15)

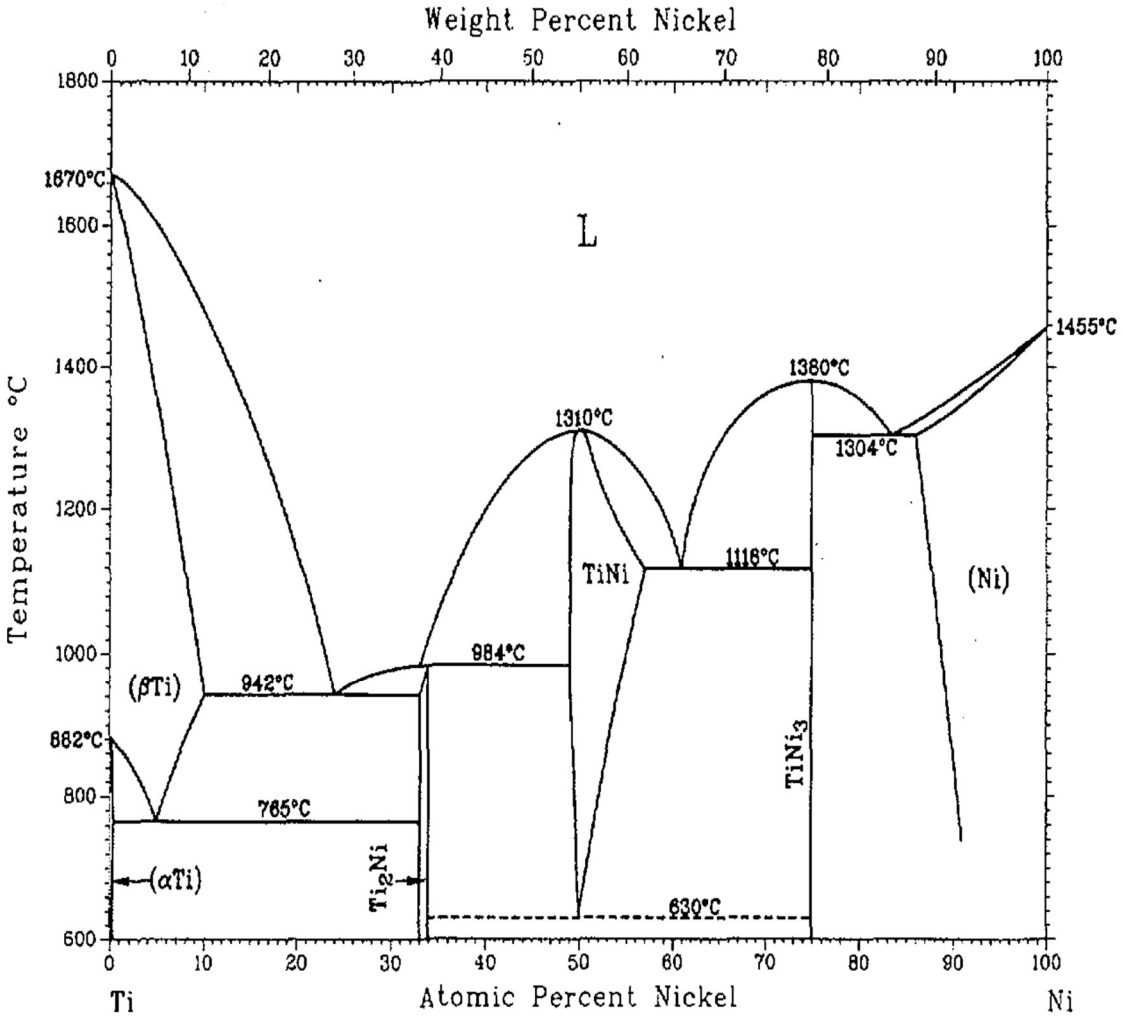

Figure 2.4: Nickel-Titanium binary phase diagram [33].

Reactions taking place during production of Ni-Ti shape memory alloys are

$$Ni + Ti \rightarrow NiTi + 67\ kJ/mol \quad \text{(Equation 2.16)}$$

$$Ni + Ti \rightarrow Ti_2Ni + 83\ kJ/mol \quad \text{(Equation 2.17)}$$

$$Ni + Ti \rightarrow Ni_3Ti + 140\ kJ/mol \quad \text{(Equation 2.18)}$$

Formation of these intermetallics are exothermic (Equation 2.16-2.18), which provides heat during sintering and makes reactive sintering possible. These exothermic reactions are called as self-sustaining. Self-sustaining reactions need heat to initiate reactions and reactions will take place by themselves after they are ignited. The ignition temperature for NiTi intermetallic is in somewhere between 877 ^{o}C and 1039 ^{o}C [34]. The ignition temperature varies with nickel/titanium ratio as well as heating cycle. Particle size changes

this temperature so that large particles, having less interface area with adjacent particles, result in rising in the ignition temperature. Having ignition temperature far lower than melting point of elemental powders and TiNi intermetallic phase makes production of shape memory alloys via reactive sintering possible.

2.6.2 Nickel Copper Phase Diagram

Unlike Ti-Ni system, which includes several intermetallics, Cu-Ni binary phase diagram (Figure 2.5) is isomorphous. Copper and nickel form complete solid solution for all compositions and temperatures. Both copper and nickel share the same crystal structure, Face-Centered Cubic (FCC). Thus, copper nickel alloys have Face-Centered Cubic structure. The only transformation is magnetic transition, which varies with nickel composition. Since the lattice parameter difference of constituents is less than 2% and they share the same crystal structure, they are soluble for all compositions [35].

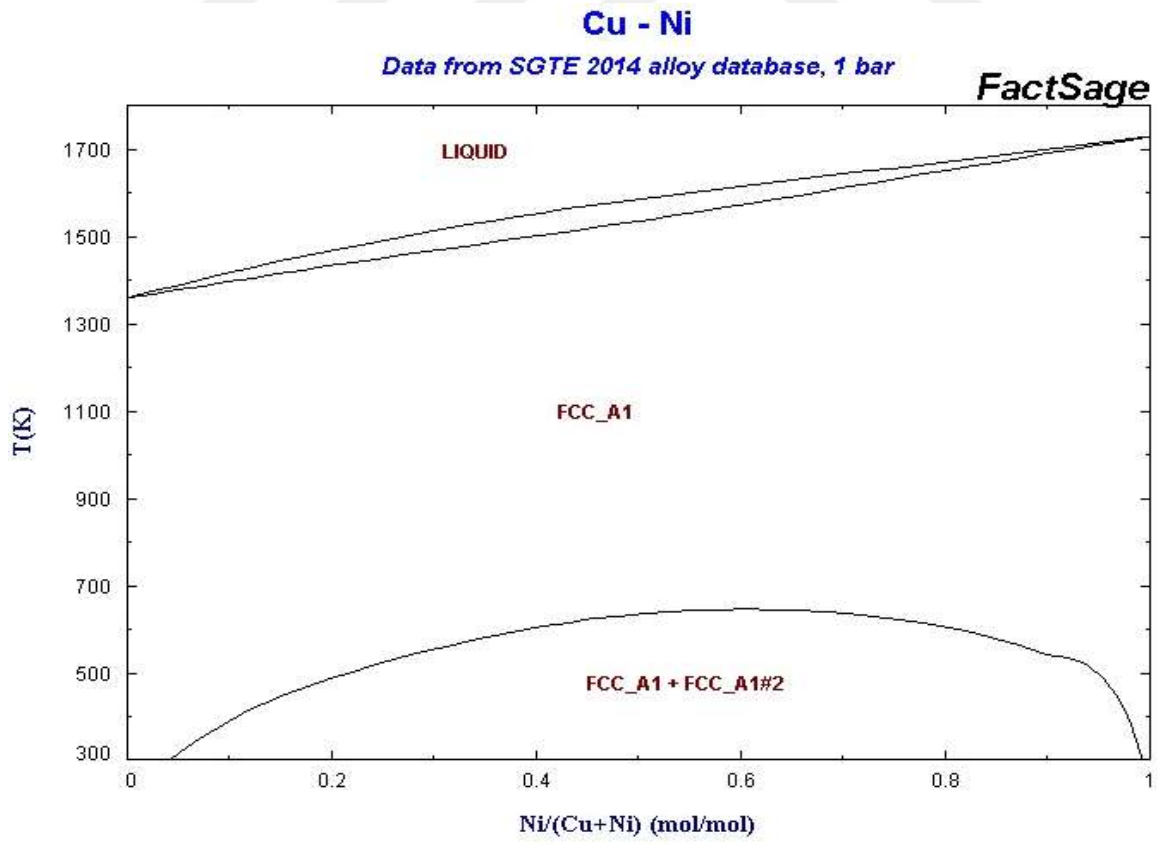

Figure 2.5: Copper-Nickel binary phase diagram [36].

2.7. Electroless Plating

Electroplating is electrochemical process in which both oxidation and reduction reactions occur simultaneously in an aqueous solution, which is called as electrolyte. During electroplating, electron transfer between reacting species leads to chemical deposition of a metal from electrolyte on the surface of the target material. Chemical deposition occurs at cathode (positively charged electrode) where reduction reaction take place by gaining electrons. On the other hand, anodic (negatively charged electrode) substance loses electrons and is consumed. In electroplating, less noble metal is plated with more noble metal until anode is fully covered with anodic substrate. As soon as cathode is fully covered, deposition rate slows down and stops. Thus, deposition thickness is thin and generally in the range of 1 to 3 microns [37]. Electroplating is applied to improve surface properties such as wear resistance and corrosion resistance.

On the other hand, higher deposition thicknesses can be achieved in electroless plating since deposition is continuous in electroless plating [38]. Electroless plating is a method in which continuous deposition takes place without use of any external electric current source [39]. Electroless plating process is described as autocatalytic, which means one of the reaction product is also a reactant [38]. Aqueous solution includes both reducing agent and substrate to be deposited, and reactions take place simultaneously as shown in Equations 2.19-2.21 [37]. Copper, gold, silver and nickel can be electroless plated on almost any substrate, including metallic and non-metallic materials [40]. Among these, nickel is widely used as electroless plating mean. Nickel plating is used in many industries such as petroleum, optics, aerospace, nuclear and food industry [41, 42].

Reduction:	$Ni^{+2} + 2e^- \rightarrow Ni^0$	E^0=-25 mV	(Eq. 2.19)
Oxidation:	$H_2PO^-_2 + H_2O \rightarrow H_2PO^-_3 + 2H^+ + 2e^-$	E^0=+50 mV	(Eq. 2.20)
Overall :	$Ni^{+2} + H_2PO^-_2 + H_2O \rightarrow Ni^0 + H_2PO^-_3 + 2H^+$	E^0=+25 mV	(Eq. 2.21)

Being one of the most important electroless plating process, electroless nickel plating solution includes source of nickel ions, reducing agent, complexing agent, and stabilizer and requires energy, which is governed by heating of solution. Nickel salts such as nickel sulphate, nickel acetate and nickel chloride are widely used as nickel ion source. Among

them nickel sulphate is the most widely used as nickel source in the form of nickel salt of hypophosphorus acid, $Ni(H_2PO_2)_2$ [37].For the reduction of nickel, four reducing agents are used; sodium hypophosphite, sodium borohydride, dimethylamine borane, hydrazine. Depending on the reducing agents used, deposit may contain phosphorous, boron or other elements, resulting in the contamination of deposition and deposition of these elements may affect the bond strength [43]. For example, phosphorous content of deposition may be as high as 13% in the form of finely dispersed phosphides. Contamination level in electroless plating is much higher than electroplating, which has purity level of 99% Ni [44].

Complexing agents used in electroless nickel plating are mostly organic acids or their salts. Commonly used complexing agents are propionate, succinate, monodentate acetate and bidentate hydroxyacetate. Complexing agents are used to retard the precipitation of nickel salts during storage at room temperature. They also keep the pH of the solution in desired level. Most of the commercial electroless nickel plating solutions have pH of around 4.5 to 6.0. High pH level is desired since the higher the pH level of the solution is, the lower phosphorous content deposits. High pH level also increases the deposition rate of electroless nickel plating [37].

In order to prevent decomposition of electroless nickel plating solution stabilizers, which are also called as catalytic inhibitors, are added in to electroless nickel plating solution. Otherwise nickel solution would decompose spontaneously not only when performing electroless plating but also during storage of the solution [45]. Even the trace of any stabilizer is enough to stop unexpected deposition on the container walls. Some examples of stabilizers are alkyl dimethylamine oxide, nitrobensinimidazole and methyl dithiouracil. Addition of these stabilizers slows down the deposition rate during plating process. However these stabilizers inhibit the deposition of nickel during storage at room temperature.

Unlike in the case of electroplating, which uses electrical energy, electroless plating consumes heat to proceed. Relation between nickel deposition thickness and temperature of the solution is Arrhenius so that deposition thickness increases exponentially with increasing temperature [37, 46]. Optimum electroless plating temperature applied

commercially is around 90-100 ºC. Temperature higher than optimum temperature may cause the boiling of the solution and consequently loss of solution.

Electroless nickel plating is used to increase corrosion resistance, wear resistance, hardness, magnetic response, solderability and thickness uniformity [47, 48]. Even though electroless nickel plating is used for many purposes, main usage of electroless nickel plating is to increase corrosion resistance of materials since nickel has very high corrosion resistance. Nickel deposits on the surface of the substrate and protects substrate from oxidation [47]. Deposition rate of nickel depends on the temperature of the solution. Deposition starts at 30 ºC and rises exponentially up to optimum electroless plating temperature which is around 90-100 ºC. Deposition rate reaches a maximum when hypophosphorus acid is used as reducing agent. As electroless plating proceeds, concentration of hypophosphorus decreases. Since hypophosphorus is reducing agent, electron source for the system, deposition rate decreases with decreasing hypophosphorus content. Thus, deposition rate is high at the beginning of the process and gets reduced as deposition proceeds.

Some metals form thick oxide layer on the surface. For example, titanium forms a tight oxide film on the surface, which reduces bond strength of electroless nickel plating. Thus, in order to increase bond strength this oxide film should be removed before plating. Copper, on the other hand, does not form a thick oxide layer so copper can be coated without removing oxide layer. However, surface to be coated must be cleaned well in order to increase bond strength and efficiency of the process [49].

2.8 Copper Nickel Alloys

Copper has very high oxidation resistance. Although copper is mostly used in electrical applications due to excellent electrical properties, such as high electrical conductivity, addition of nickel makes copper one of the best alloy for corrosive environment such as salty water environment. Copper, which has a high degree of nobility, and nickel, which is able protect itself from oxidation, alloys are resistant in both reducing conditions and oxidizing conditions [50]. Alloys of these elements have better corrosion resistance than pure form of both copper and nickel. Not only corrosion resistance but also mechanical properties of alloy can also be enhanced. For example, addition of 1.5% Ni can double the

impact toughness, and other mechanical properties such as fatigue, yield and tensile strength can also be improved [51]. Maximum strength is achieved when nickel concentration is approximately 70% [52].

Copper nickel alloys have excellent corrosion resistance. They can even withstand sulphuric, hydrochloric, hydrofluoric and phosphoric acid which are very corrosive for many alloy systems [51]. They are resistant to not only liquid attacks but also gaseous attacks at room temperature. Since copper nickel alloy forms complete solid solution for all composition of nickel and copper, they exhibit excellent ductility and impact toughness even at -78 ^{o}C [53]. Some applications of these alloys are chemical processing equipment, heat exchangers, vessel, piping, electrical and electronic components. Electrical resistivity and strength decreases with decreasing nickel content.

Although nickel-copper alloys are mostly used for their excellent corrosion resistance, alloy containing 45% nickel, which is known as constantan, is used as thermocouple element [54]. It has higher thermal emf (electro motive force), difference in potential, than platinum [55]. This alloy is also used as heating element since it has the highest electrical resistivity among all nickel-copper alloys. In addition, these alloys are useful for recording magnetic data and sensor thanks to the giant magneto resistance effect, quantum mechanical magneto resistance effect.

Cu-Ni alloys are mostly produced as cast and then they are rolled. However, as the nickel content increases, tendency of gas absorption increases [56]. During solidification of the alloy solubility limit for gases such as oxygen and hydrogen decreases and as a result micro pores form and as a result decreases the mechanical, and electrical properties of the alloy. On the other hand, powder metallurgy offers low gas pore formation.

2.9 Shape Memory Alloys

Shape memory alloys (SMAs) are alloys that remember their initial shape (pre-deformed shape) after deformation at low temperature and turn back their initial shape upon heating. This phenomenon is called as shape memory effect. They can also recover their initial shape after deformation by mechanical loading above austenite finish temperature (A_f), which is called as psuedoelasticity or superelasticity. In shape memory alloys, two phases

exist: martensite and austenite. While austenite, which is generally cubic, is high temperature phase, low temperature phase is martensite, which can be tetragonal, orthorhombic or monoclinic. Phase transformation between martensite and austenite is displacive, which does not occur by diffusion but shear [57]. Shape memory effect and superplastic effect arise from this diffusionless phase transformation between martensite and austenite phases. In addition, this transformation is reversible and does not involve volume change, unlike the martensitic transformation in Fe-C system [58]. Thus, martensitic transformation in shape memory alloys takes place via twinning, which does not cause any volume change during phase transformation. Buehler et al. [59] firstly found shape memory effect in 1963 in Ti-Ni system with an equimolar composition, which is known as NiTiNOL. Although many alloy systems, such as Ag-Cd, Au-Cd, Fe-Mn-Si and Mn-Cu, have been found to have shape memory effect since the discovery of Ni-Ti, Ni-Ti system is the most important one due to its excellent mechanical properties [58].

2.9.1 Shape Memory Effect and Superelasticity

At low temperatures shape memory alloys have twinned martensitic phase. After loading, this twinned martensitic phase transforms in to detwinned martensite. When detwinned martensite is heated above A_f, detwinned martensite transforms in to austenite and SMA regain its initial shape as seen in figure 2.6. This Shape Memory phenomenon is called as “thermoelastic martensitic transformation”. Since shape recovery can be achieved by only heating, this is known as “one way shape memory effect”. Specific thermomechanical treatment, so called training, of SMAs causes “two way shape memory effect” in which SMAs remember both martensitic and austenitic shapes. In other words, only changing the temperature of the alloy results in shape change of alloy without external stress.

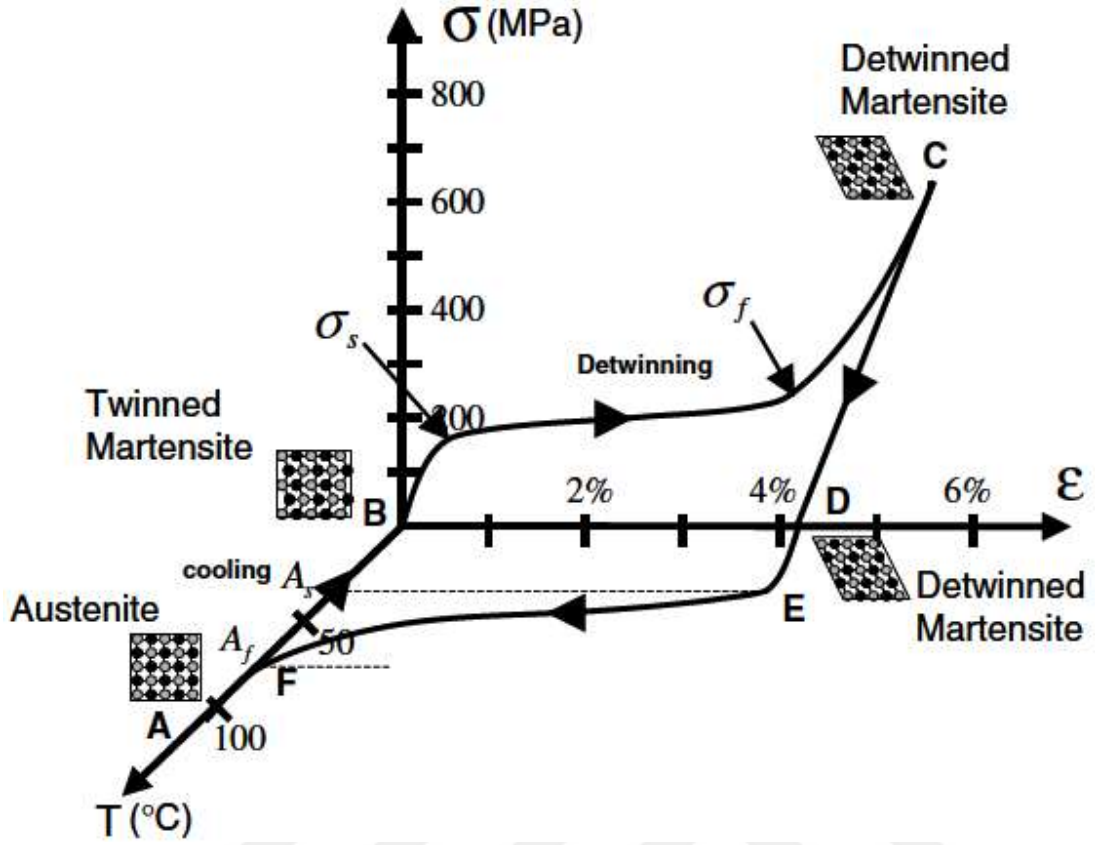

Figure 2.6: Stress-strain-temperature data exhibiting the shape memory effect for a Ni-Ti SMA [58].

Superelasticity, or psuedoelasticity, observed at temperatures above A_f. Applying stress above A_f causes stress-induced martensitic transformation. This transformation is reversible so that upon unloading unstable detwinned martensite formed during loading transforms into austenite.

2.9.2 Titanium-Nickel Shape Memory Alloys

Ti-Ni based shape memory alloys' microstructure consist of single phase NiTi and small amount of other intermetallics. Formation of these intermetallics are unavoidable because stoichiometric range of NiTi narrows with the decreasing temperature. Small changes in the composition of the alloy result in the precipitation of coarser intermetallics, which effects the hot workability of the alloy. Composition change also affects the martensite start temperature (M_s) so that increasing Ni content from 50% to 51% lowers the M_s by around 80 °C [60].

Conventionally, Ni-Ti shape memory alloys are cast and then rolled into desired shape or machined. Casting of SMAs are done under high vacuum or inert gas atmosphere in order to prevent alloy from oxidation. However, being a near net shape production route, powder metallurgy offers production of SMAs. Moreover, it is possible to produce shape memory alloys for some specialized applications such as porous implants. Ti-Ni shape memory alloys are widely used in medical applications since they have high biocompatibility. Pores present in the alloy allow the growth of cells.

CHAPTER 3

METHODOLOGY

In this chapter, raw materials and experimental procedures which are used in this project are described in details. In the first section materials used, their compaction and sintering procedure are presented as well as preparation of final sinters for characterization are described. Experimental set up for electroless nickel plating are described as well. In the second section, characterization techniques used in this project are given.

3.1 Materials and Methods

3.1.1 Raw Materials

High purity Titanium (purity 99.9%), Nickel (purity 99.8%) and Copper (purity 99.5%) powders with a size of -150 mesh obtained from Alfa Aesar were used in this project. As sintering of fine particles is better than coarse particles, fine powders were selected in order to improve efficiency of the sintering process. Equimolar Titanium-Nickel and equimolar Copper-Nickel powders were mixed and then pressed in to pellets, whose diameter is 10 mm and thickness is around 4-5 mm by using automatic Speca Press, uniaxial hydraulic laboratory press. Approximately 2 grams of each powder mix were

pressed with the pressure of 500 MPa. Powders were kept at this pressure for 5 minutes to obtain well bonded green bodies. Densities of powders were calculated by using ρ=m/V, where m is mass and V is volume. Average green density of equimolar nickel-titanium compact was 4.93 g/cm^3, which corresponds to 75% of theoretical density. On the other hand, average green density of equimolar nickel-copper was 7.62 g/cm^3, which corresponds to 85% of theoretical density.

3.1.2 Preventing Pellets from Oxidation

Sintering was performed in Carbolite box furnace, which operates under atmospheric condition. In atmospheric furnace main concern is the reaction between compacted green bodies and oxygen. Thus, in order to prevent pellets from oxidation, which is expected to affect the sintering process, pellets were placed into alumina and nickel crucibles as seen in Figure 3.1. Alumina powders were placed in the crucibles first. Alumina powders were used because of the fact that alumina is thermodynamically very stable and does not react with the other compounds used in this project at the sintering temperature. Pellets, then, were embedded into thick layer of alumina powders so that effect of oxidation can be reduced to a minimum level. Crucible was closed with an alumina lit so as not to let air flow in the crucibles. Furthermore, titanium sponge is poured on the alumina powder since titanium has high oxygen solubility at high temperatures (titanium can dissolve around 7 at. % oxygen at the sintering temperature). Titanium sponge is placed to dissolve oxygen present in the crucible.

Figure 3.1: Prevention samples from oxidation.

3.1.3 Sintering

A Carbolyte atmospheric box furnace was used in order to perform sintering process. Green compacts, which were placed in to alumina and nickel crucibles, are put in to preheated furnace, which accounts for heating rate of around 300 ºC/min. For copper-nickel system, sintering operation was performed at 900 ºC (83 per cent of absolute melting point of copper). These samples were held in the furnace for 1, 2, 4 and 8 hours. On the other hand, sintering of titanium-nickel green bodies was performed at two different temperatures, at 900 ºC and 1000 ºC. These temperatures were selected to investigate the formation of different intermetallics at different temperatures since Nickel-Titanium phase diagram suggests that there is a eutectic transformation at 942 ºC, above which Ti_2Ni is not thermodynamically stable. Moreover, Novak et al. [61] investigated formation of intermetallics in Ni-Ti system below 900 ºC and they could not observe formation of any intermetallics. Thus, 900 ºC was chosen as minimum sintering temperature for Ni-Ti system. Samples were held at these temperatures for 1, 2, 4 and 8 hours. Following sintering operation, furnace turned off so that pellets were furnace cooled. Dimensions and weights of sintered pellets were measured in order to calculate final density of the pellets.

3.1.4 Sectioning of Samples

Sintered samples were cut into two halves with a diamond saw (IsoMet 1000 Precision Cutter, Buehler Ltd.) in order to investigate the inner cross section of the samples. Following sectioning, samples were hot mounted in bakelite by using Simplimet 1000 automatic hot press mounting machine.

3.1.5 Grinding and Polishing

In order to investigate microstructure of the samples in optical microscope and Scanning Electron Microscope (SEM), samples were grinded and polished. Grinding was performed in Buehler Metaserv 250 Twin semi-automatic machine using silicon carbide grinding media. Starting from 120 grit size, samples were grinded on 240, 320, 600 and 1200 grit sizes. After every grinding operation, samples were plunged in to ultrasonic bath and washed for 1 minute in order to remove particles stuck on the surface of the samples during grinding. Samples, later, were polished by using 6 and 3 μm diamond solution and dried.

3.1.6 Etching

Etching of nickel-titanium was performed by using hydrofluoric acid solution. Nickel-copper sinters were etched by using nitric acid solution.

3.1.7 Electroless Nickel Plating

Electroless nickel plating solution supplied by Alfaeaser was used for electroless plating of titanium and copper powders. 100 ml of electroless solution was poured into glass crucible. Solution, then, was put on hot plate and heated to 90 ºC. A thermometer is immersed in to solution to read the temperature of the solution and to ensure that temperature of the solution was being kept around 90 ºC. When the temperature of the solution was reached, 10 grams of copper powder was added in solution. During electroless plating, solution was well stirred so that powders do not agglomerate and were fully nickel-plated. Copper powders were held in the solution for 3 hours. Following that, powders were taken out from solution and washed in order to reduce contamination of powders and to remove the remaining of electroless plating solution. Following cleaning of powders, powders were dried for 2 days under atmospheric conditions. Same procedure was applied to 20 gr titanium powders but 200 ml of solution was used instead of 100 ml solution. After electroless nickel plating, nickel plated powders (without any nickel powder addition) were pressed under 500 MPa of pressure, which is the same pressure as used in non-plated powders by Speca Press, uniaxial hydraulic laboratory press. Compacts, then, sintered same as the non-nickel-plated powders.

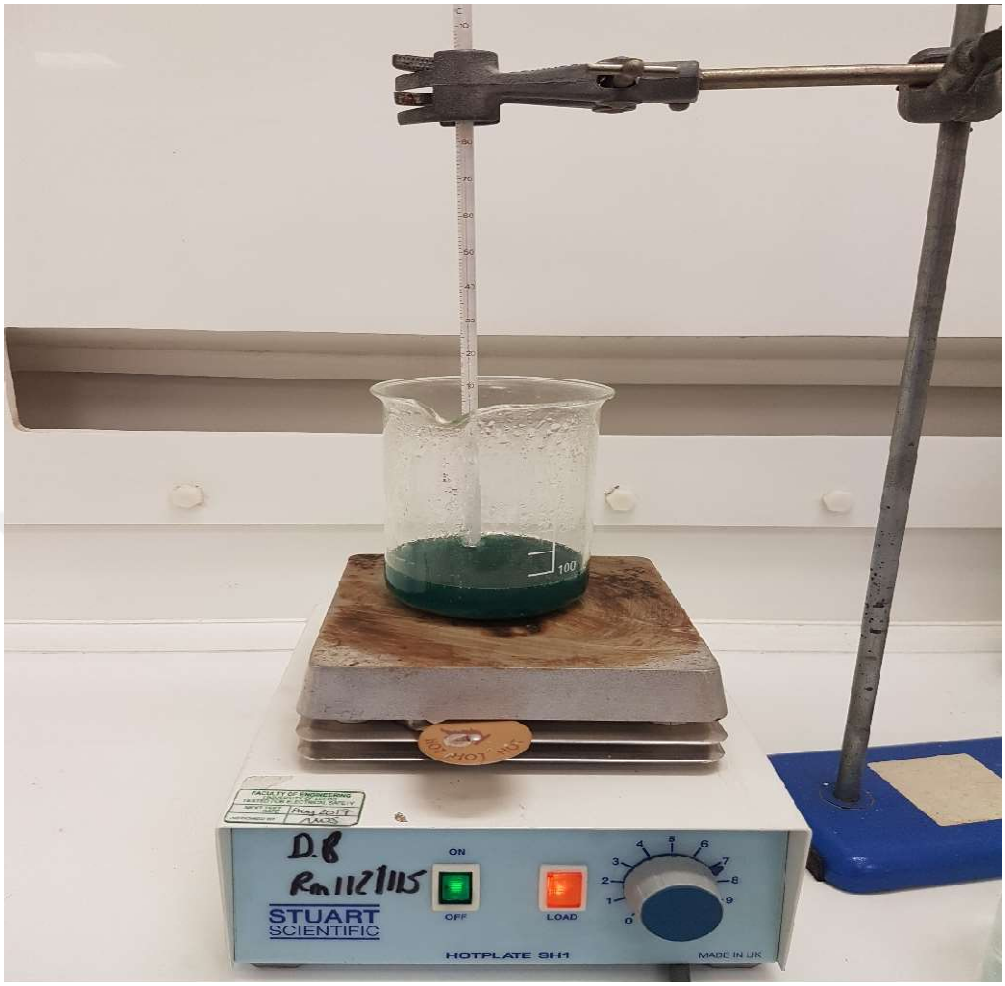

Figure 3.2: Electroless nickel plating, experimental set up.

3.2 Characterization of Samples

Characterization of samples were done by using optical microscope, Scanning Electron Microscope (SEM) and X-Ray Diffraction (XRD). Pore fraction of the samples were calculated by using ImageJ software.

3.2.1 Optical Microscope

Optical microscope was used to measure the thickness of electroless nickel coating. Nickel plated powders were mounted in bakelite by using Simplimet 1000 automatic hot press

mounting machine. Mounted powders, then, grinded and polished by using Buehler Metaserv 250 Twin semi-automatic machine. Mounted powders were placed in optical microscope and examined using bright field imaging technique.

3.2.2 Scanning Electron Microscope

Samples were analysed by using EVO MA15 Scanning Electron Microscope (SEM) and Hitachi Desktop SEM. Since SEM produces images by scanning the surface of a material by using accelerated electrons, the surface of the sample must be conductive. Otherwise, there will not be electron flow from filament to sample, as the electrons would pile up on the surface of the specimens. Thus, samples were carbon coated by using Quorum 150T carbon coating machine in order to make samples conductive. Carbon coated samples, then, placed into SEM and air inside vacuumed. Backscatter imaging technique, which shows lighter elements darker and heavier elements brighter, was used in order to identify elemental powders. Using Energy-Dispersive X-Ray Spectroscopy (EDX), elements present in samples were observed. In addition, EDX was used to get elemental mapping of each sample.

3.2.3 Pore Fraction Calculation

Backscatter SEM images were also used to calculate pore fraction (two dimensional) of non-plated samples. To do this, a software named ImageJ was used. This software converts images in to binary images, which is two-coloured image; black and white (Figure 3.3). Binary image has only two possible values. In binary image while black regions show the pores, white regions show the matrix. Software then calculates the fraction of each area represented by black and white colours. For each sample, calculations were made two times and average of these data was used.

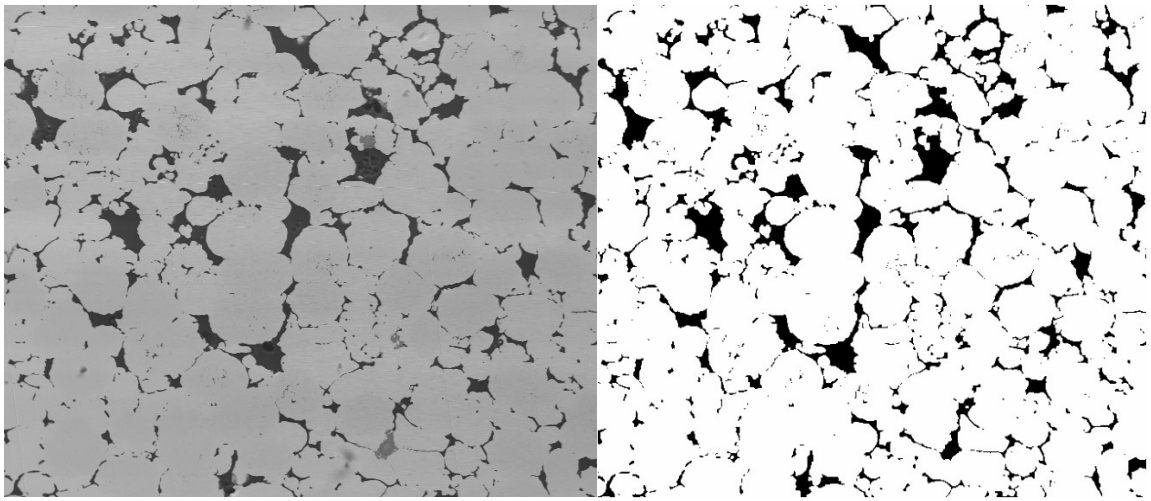

Figure 3.3: SEM image (left) and binary image converted form SEM image by using ImageJ (right).

3.2.4 X-Ray Diffraction

X-Ray Diffraction (XRD) gives information about phases present in samples and crystal structure of the samples. XRD was used in order to detect the phases present in samples. XRD was used to characterize only Ni-Ti samples since Ni-Cu system forms complete solid solution for all composition range. Analysis were made at diffraction angles from 20º to 80º. Instrument used for XRD analysis was Bruker D8 Diffractometer. XRD was done by using monochromatic copper Kα which has a wavelength of 1.5406 Å. XRD data collected and sketched on Excel and peaks were compared by using ICDD (International Centre for Diffraction Data) Powder Diffraction File (PDF) cards of phases present in the Ti-Ni phase diagram.

CHAPTER 4

RESULTS AND DISCUSSION

4.1 Results

4.1.1 Pore Fraction Change

During sintering of powder mixtures, pores fraction between powder compacts decreased. As discussed in Chapter 2, sintering time and sintering temperature has an influential effect on closure of the pores so that as the sintering time and sintering temperature get higher and longer, fraction of the pores is expected to get lower. That is because of the fact that densification due to transport mechanisms takes place. However, higher temperature and dwell may result in the extensive grain growth. Pores present after sintering effect the mechanical properties of the final product. After examining the polished samples of Cu-Ni, pore fraction of samples were determined. SEM backscatter images converted into binary images and fraction of the pores are determined as explained in Chapter 3. Binary images of 1 hour and 8 hour sintered Cu-Ni powder mixture are given in Figure 4.1 and Figure 4.2, respectively.

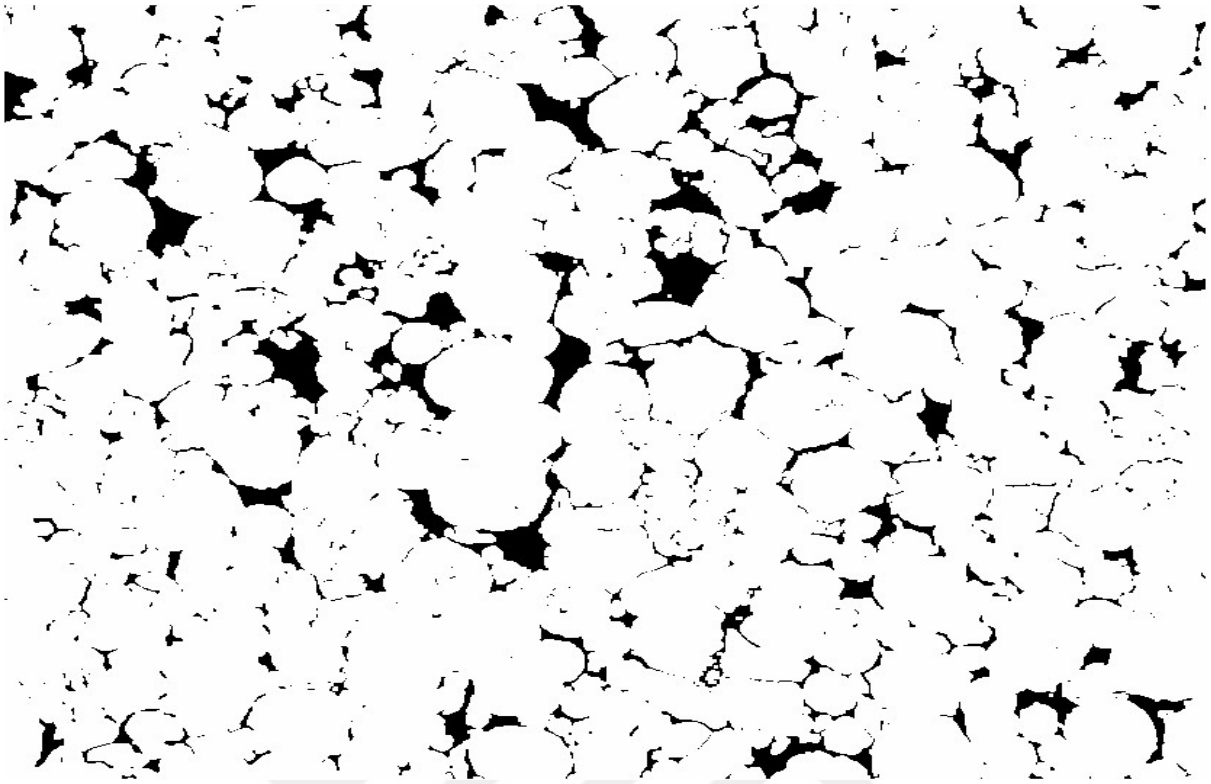

Figure 4.1: Binary Image of Cu-Ni sample sintered for 1 hr at 900 ºC showing pores (in black).

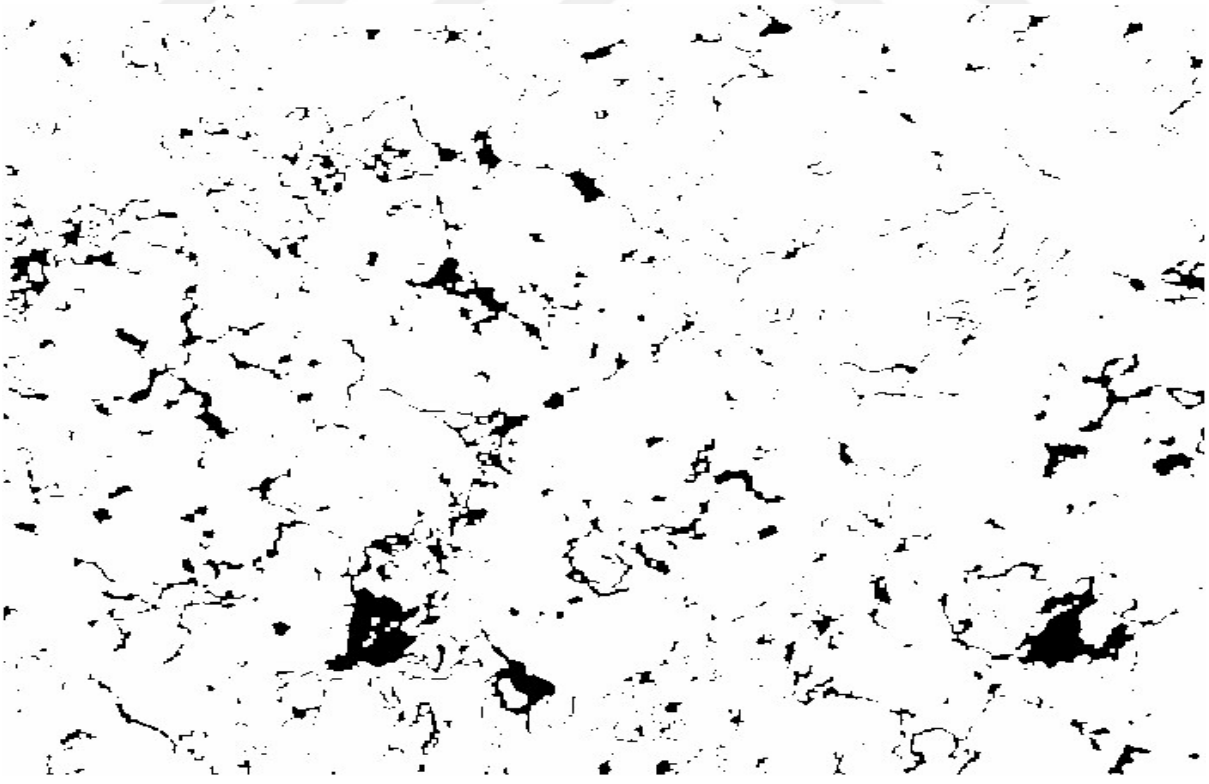

Figure 4.2: Binary image of Cu-Ni sample sintered for 8 hr at 900 ºC. Pores are shown in black.

Figure 4.3 shows the relation between pore fraction and holding time. While the pore fraction of 1 hour sintered Cu-Ni (50 at%) is 8.48 %, higher sintering time reduced this ratio so that 8 hour sintering resulted in decreasing pore fraction to 3%. As the figure 4.3 suggests pore reduction followed a linear decrease and this linear decrease is given in the graph.

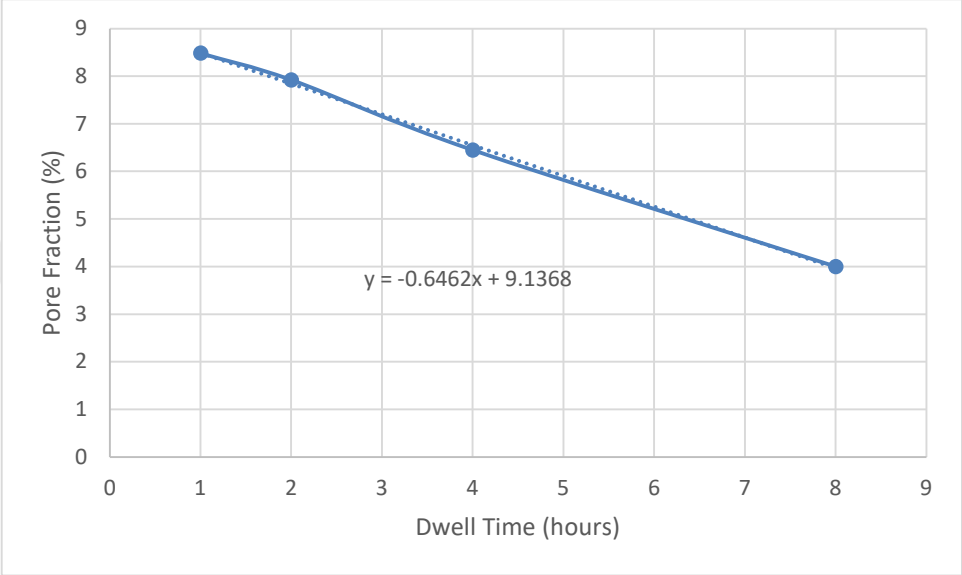

Figure 4.3: Pore fraction change in Cu-Ni powder mixture.

SEM images of Ti-Ni sinters were also investigated by using Imagej software. Fraction of pores were calculated. Unlike Cu-Ni, which showed a linear pore fraction decrease as the sintering time increases, pore fraction of Ti-Ni system was fluctuated (Figure 4.4). Ti-Ni powders sintered at 1000 ºC for one hour had a pore fraction of 21% and this ratio increased to 28% for sintering of 2 hours. Pore fraction gets the lowest value, 20%, when sintering time was 8 hours. Sintering of TiNi at 900 ºC has shown a similar pattern so that pore fraction increased from 20.23% to 26.23% between 1 and 2 hours of sintering. Pore fraction, later, decreased to 21.2% as the sintering time is 8 hours. There are two reasons for increase in porosity in Ni-Ti system: formation of Ni_3Ti and Kirkendall Effect [61]. Formation of Ni_3Ti increases the porosity of sinters.

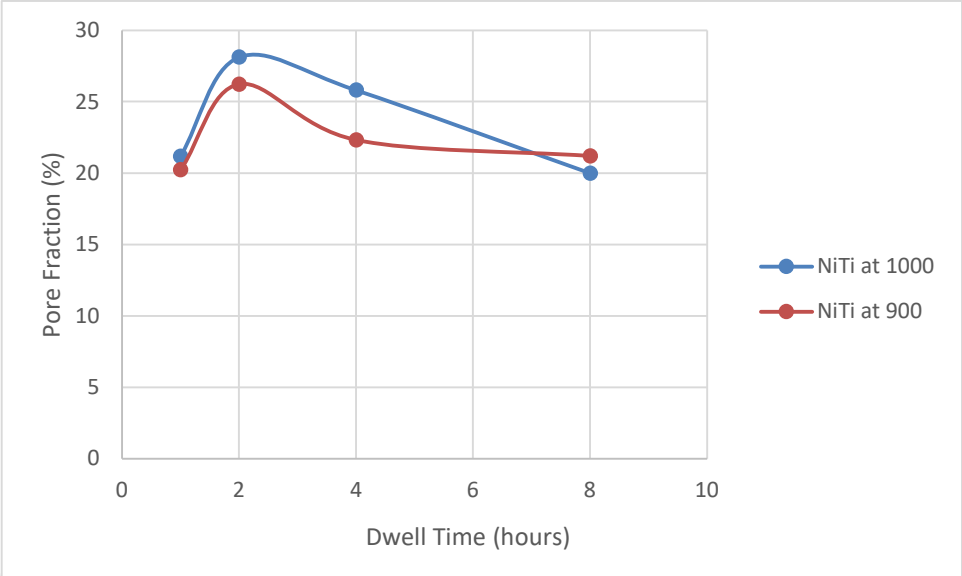

Figure 4.4: Pore fraction change in Ni-Ti powder mixture.

4.1.2 Volume Change of Sinters

In order to observe density change of sintered pellets, their initial and final densities were calculated. Sintering temperature and time change the density of the final sinter. Since powder metallurgy is near net shape production route, dimensional precision of sintered parts becomes crucial. Dimensional change of sinters depend on several factors such as particle size, composition of mixture, sintering time and temperature. In this project, Cu-Ni powder mixture was sintered at 900 ºC for 1, 2, 4 and 8 hours. Effect of sintering time on volume change was also investigated.

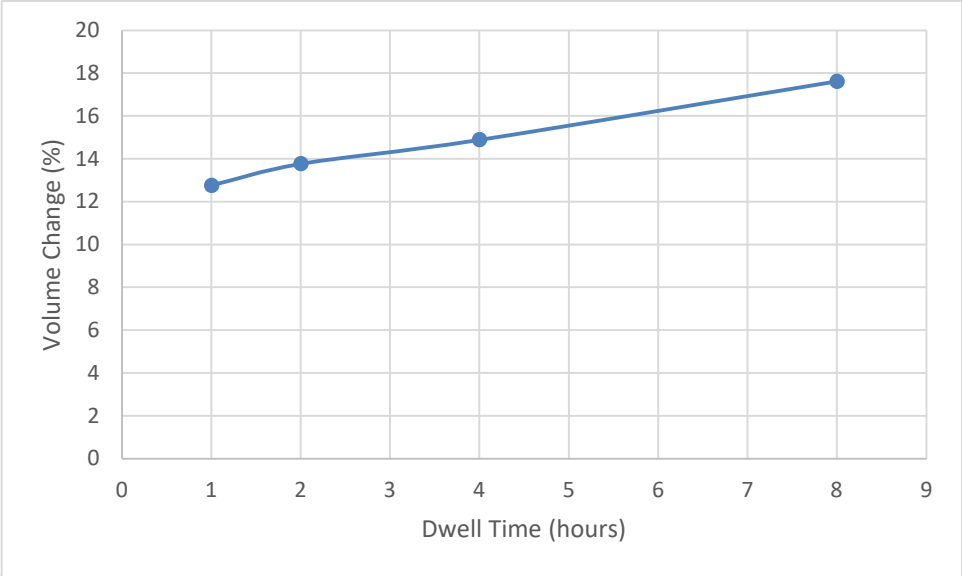

Figure 4.5: Volume change of Cu-Ni powder mixture.

Figure 4.5 shows the volume change of Cu-Ni powder mixture sintered for 1, 2, 4 and 8 hours. Volume of the sinters were increased from 12.75% to 17.6% linearly. Longer sintering times resulted in the increase of volume. It is noteworthy that largest volume change rate observed when the sintering time is 1 hour so that 1 hour sintering resulted in 12.75%. Later this rate decreased.

Similarly, longer sintering time increased the volume of the sinters in Ni-Ti mixtures (Figure 4.6). Volume change rate decreased as sintering time increased. Different sintering temperature did not make any significant difference in the volume change of sinters. Ni-Ti mixture sintered at 900 ºC and at 1000 ºC followed a parallel volume change. Thus, it can be concluded that sintering at given temperatures does not make any change when it comes to volume change for Ni-Ti mixture.

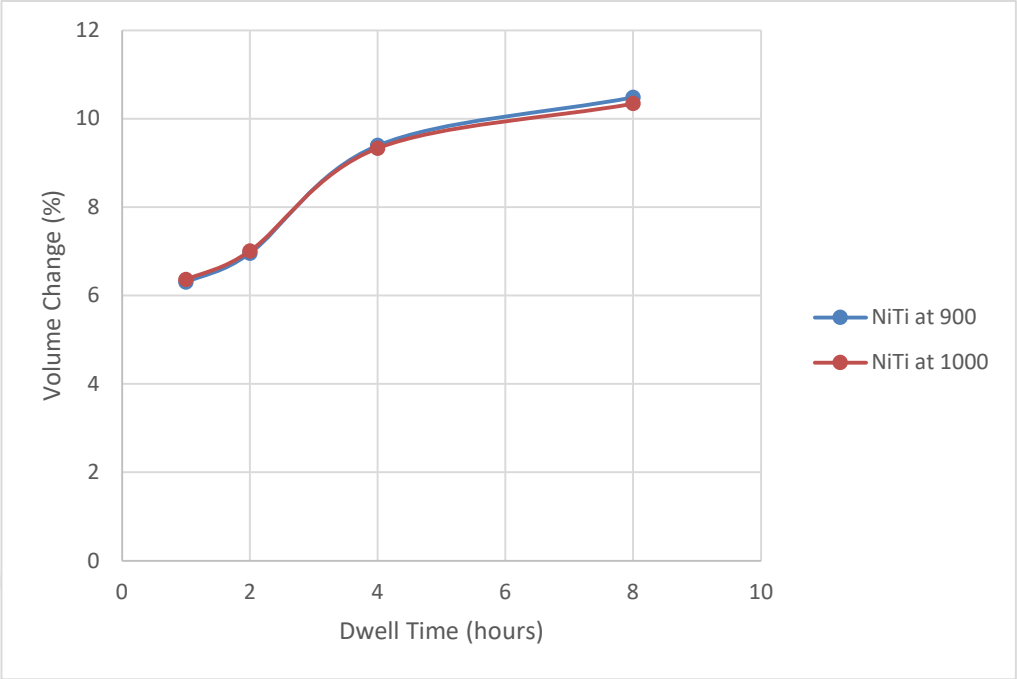

Figure 4.6: Volume change of Ni-Ti powder mixture.

As the volume of both Ni-Cu and Ni-Ti systems increased, density of these systems decreased. In other words, pellets got expanded instead of shrinking. The difference in volume change between Ni-Ti and Ni-Cu is probably due to the formation of intermetallics in Ni-Ti system.

4.1.3 XRD Analysis

As explained in previous chapter, X-Ray Diffraction (XRD) was used to investigate the phases formed during sintering of Ti-Ni powder mixture. In order to identify the phases, results taken from XRD machine were sketched on Excel. Phases matched by using Powder Diffraction File (PDF) cards. Figure 4.7 shows XRD pattern of Ti-Ni powder mixtures sintered for 4 hours at 900 ºC. Phases present for this sample are Ti, Ni, NiTi and $TiNi_3$. Similarly, samples sintered at 1000 ºC have the same XRD pattern (Figure 4.8), which shows that same phases formed during sintering at 1000 ºC. Presence of Ti and Ni phases in XRD data indicates that sintering of powder mixtures were not completely formed intermetallics. Since XRD peaks of Ti and Ni is very high as compared to other phases formed during sintering, it can be said that only small amount of powders reacted to form intermetallics. In other words, amount of intermetallics formed was low.

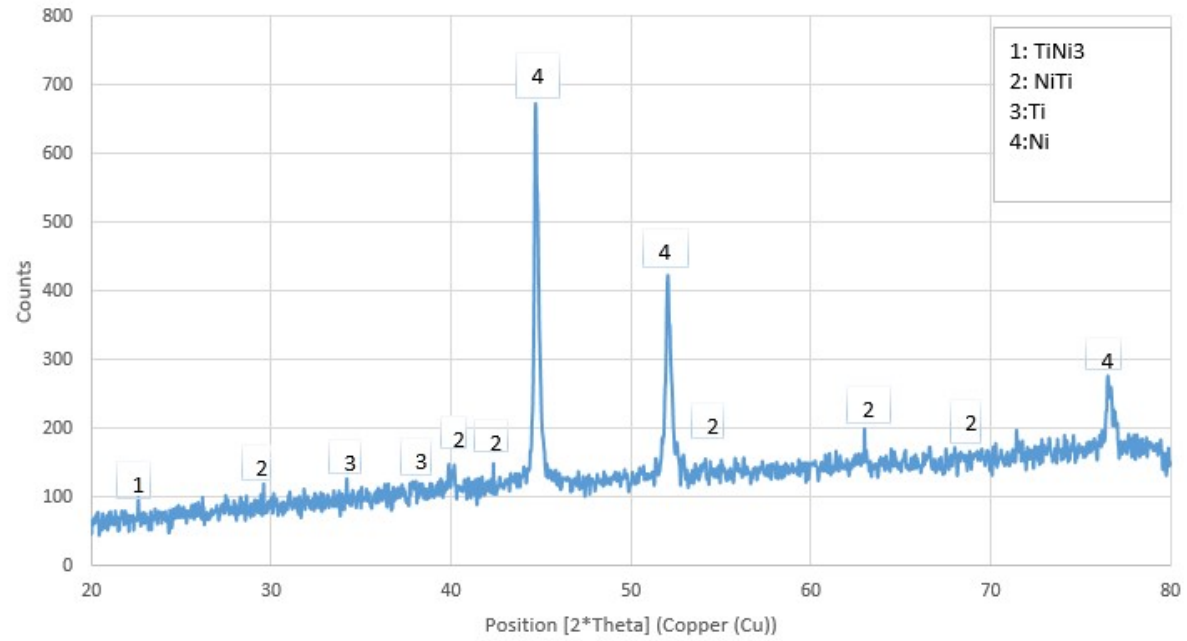

Figure 4.7: XRD of sintered and polished Ti-Ni powder mixtures containing Ti, Ni, NiTi and $TiNi_3$ (sintered 4 hours at 900 ºC).

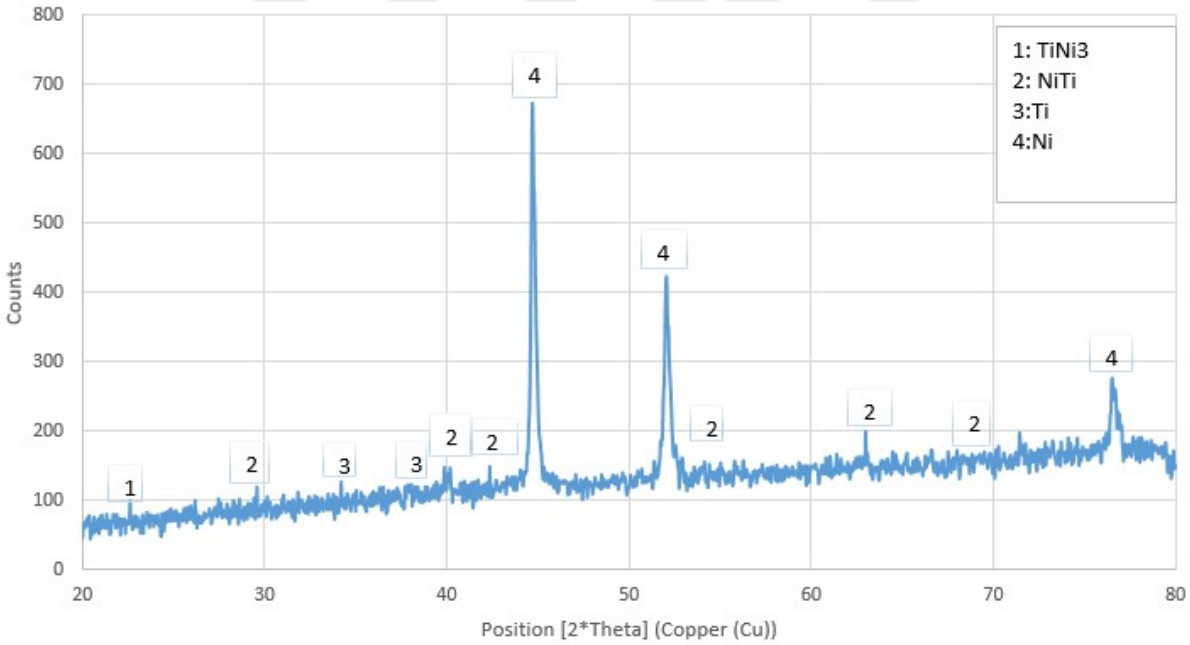

Figure 4.8: XRD of sintered and polished Ti-Ni powder mixtures containing Ti, Ni, NiTi and $TiNi_3$ (sintered 4 hours at 900 ºC).

4.1.4 SEM Analysis

Morphologies of the sintered samples were investigated from SEM images. Figure 4.9 shows microstructure of sample sintered at 900 ºC for 4 hours and elemental mapping of the sample. As seen from the figure, titanium powders bonded together as well as nickel powders. However, it is clear from the figure that nickel and titanium powders formed a boundary like structure at the interface. In other words, there seems no bonding between adjacent titanium and nickel powders. As XRD results suggest NiTi and $TiNi_3$ formed during sintering. Thus, it can be said that these intermetallics are formed at the interface of the powders and later formation of intermetallics stopped. They acted as barrier for further diffusion.

Novak et al [62] investigated formation of intermetallics in Ni-Ti system and found a similar result. They concluded that since reaction between nickel and titanium is diffusion-controlled, intermetallics formed inhibits the diffusion of nickel and titanium. Formation of nonstoichiometric NiTi intermetallic, which has strong bonding forces, at the interface inhibited the diffusion of both titanium and nickel. They also found that lower heating rates (<20 ºC/min) form intermetallics at the surface and inhibits the further diffusion of elements [63]. Lower heating rates promote the formation of intermetallics at the interface and these intermetallics acted as diffusion barrier and prevented reactive sintering of Ni-Ti system. While a small amount of nickel diffused in to titanium (Figure 4.9) no traces of titanium is present in nickel powders. Divinski et al. [64] calculated the diffusivities of Ni and Ti in B2 NiTi. They found that Ni diffuses faster than Ti in NiTi by two orders of magnitude. Similarly, in the case of sintering at 1000 ºC, intermetallics formed at the interface slowed down the diffusion of species. Comparing diffusivities of nickel in β-Ti [65] and NiTi [64] at 900 ºC gives that nickel diffuses 100 times faster in β-Ti.

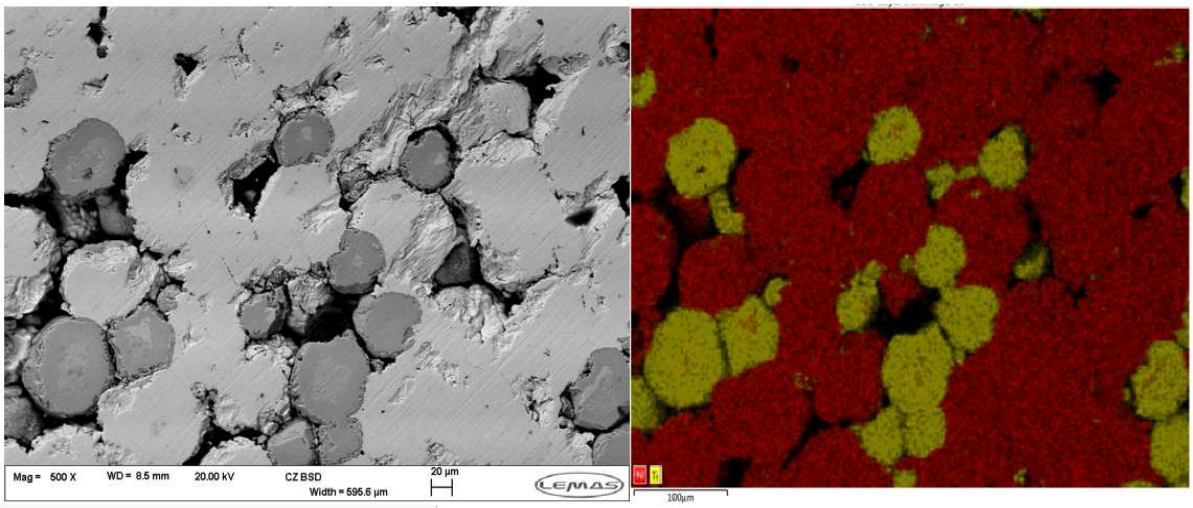

Figure 4.9: SEM back scatter image (left) and elemental mapping (right) of the same sample sintered at 900 ºC for 4 hours showing elements (Ni in red, Ti in yellow).

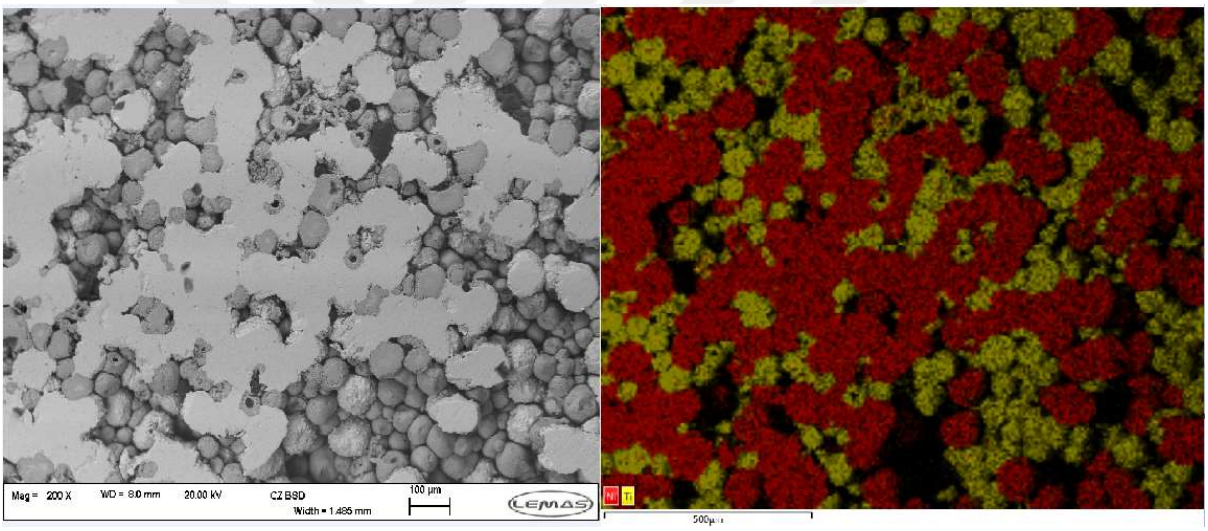

Figure 4.10: SEM back scatter image (left) and elemental mapping (right) of the same sample sintered at 1000 ºC for 4 hours showing elements (Ni in red, Ti in yellow).

Figure 4.11 shows the microstructure of Cu-Ni sintered for 1 hour (left) and 8 hours (right) at 900 ºC. SEM image on the right shows that copper and nickel powders bonded together. Although they formed bonds, time for diffusion was not enough to form a complete solid solution same as the samples sintered for 2 and 4 hours. Sintering for 8 hours resulted in the formation of complete solid solution for copper nickel system. Thus, time needed to form complete solid solution at 900 ºC is somewhere between 4 and 8 hours. While centre of Cu-Ni pellets bonded after 4 hours of sintering, parts close to the surface took longer

time to get bonded. This can be due to nonuniform distribution of stress resulting from pressing of powder mixtures.

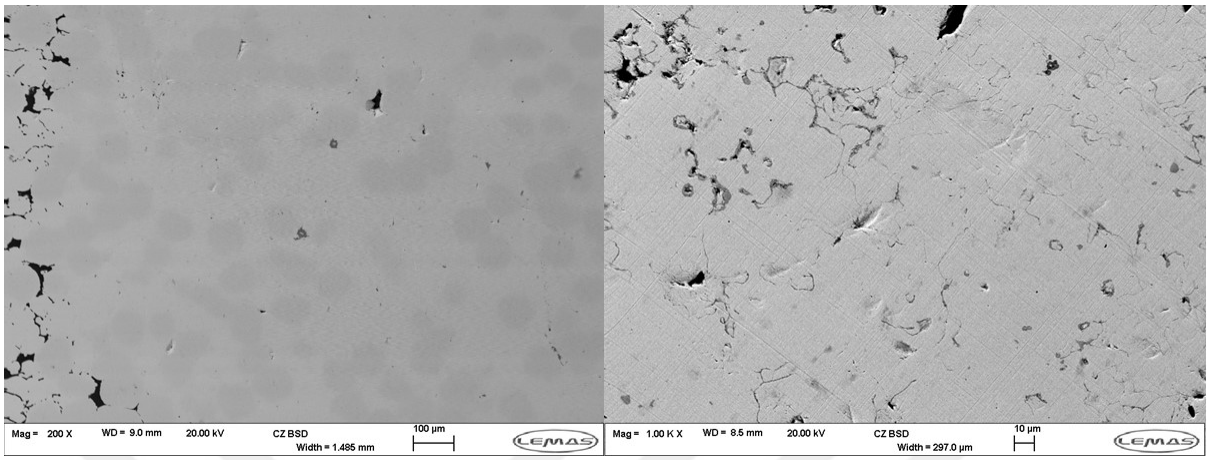

Figure 4.11: SEM backscatter image of Cu-Ni sintered at 900 ºC for 1 hour (left) and for 8 hours (right).

4.1.5 Electroless Nickel Plating

Titanium and copper powders were electroless-nickel plated by keeping the powders in heated electroless nickel plating solution supplied by AlfaAesar for 3 hours and then sintered as explained in chapter 3. Measurement of thickness of electroless nickel plating is an important issue since it decides the composition of final powder. Thus, thickness of electroless plating was measured under optical microscope after mounting and polishing the electroless-nickel plated powders. Thickness for electroless plating was around 3.7 micrometre (Figure 4.12).

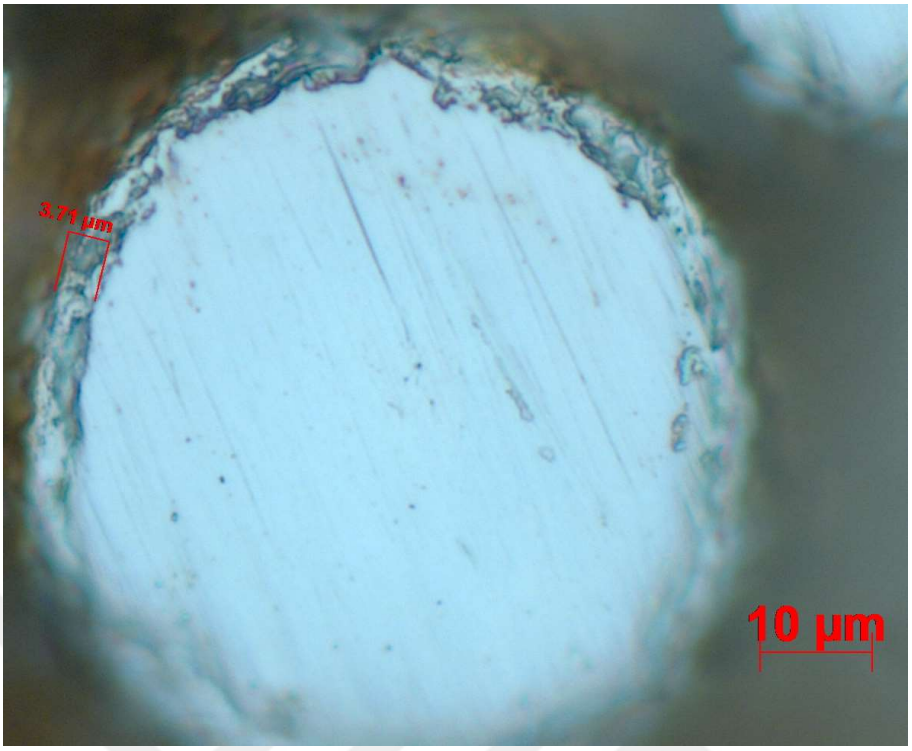

Figure 4.12: Electroless-nickel plated titanium powder with plating thickness of 3.71 micrometre.

Electroless-nickel plated and sintered samples were investigated by XRD as explained in Chapter 3. Figure 4.13 show phases present in sample sintered at 900 ºC for 4 hours. There present $TiNi_3$, TiO_2, NiTi and Ti phases. Sintering at 1000 ºC showed same result so that phases present in the sinters were the same except formation of rutile (TiO_2). In non-plated powders there seem no evidence of formation of rutile. However, in electroless-nickel plated powders rutile was formed. As explained in chapter 2 on the surface of metal powders oxygen is present. After electroless plating of powders oxygen was stuck between nickel and titanium, and was not able to leave the system due to presence of nickel on the surface.

When compared to non-plated samples, electroless-nickel plated samples formed more intermetallics since peak intensities for intermetallics are higher in electroless plated powders. This is due to the fact that electroless-nickel plating provides more surface for diffusion, on which formation of intermetallics takes place. In both electroless plated and non-plated samples, intermetallics present were nickel rich intermetallics, TiNi and $TiNi_3$. Titanium rich intermetallic, Ti_2Ni, did not form in neither plated nor mixed powders.

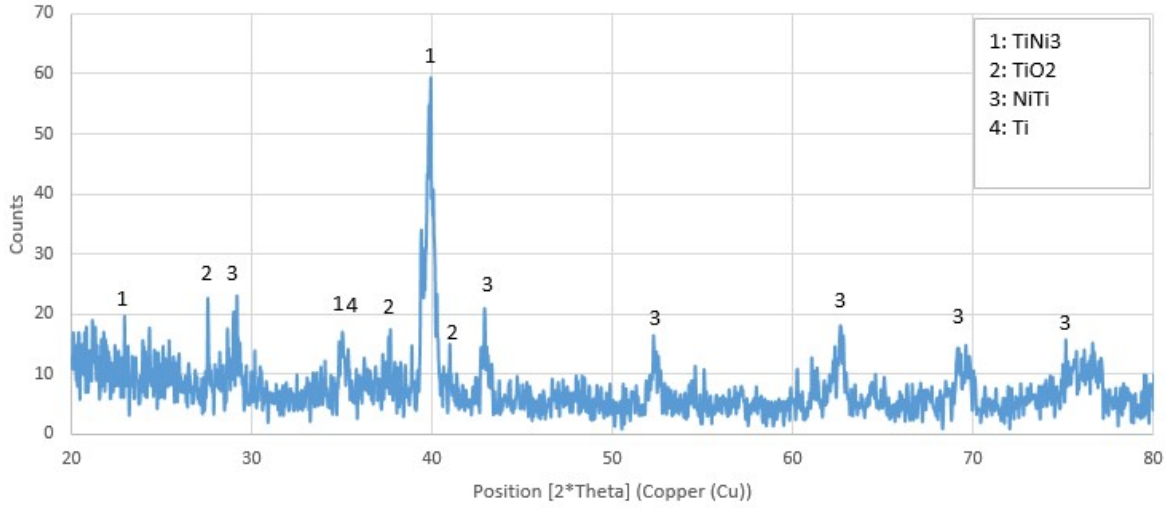

Figure 4.13: XRD pattern of electroless-nickel plated and polished sample containing $TiNi_3$, TiO_2, NiTi and Ti (sintered at 900 ºC for 4 hours).

SEM backscatter image for nickel-plated and sintered sample for 4 hours is given in Figure 4.14. Intermetallics formed along some parts of the surface of the titanium powder. This figure also shows that electroless nickel plating did not result coating of whole powder since intermetallics were not formed all around the surface of titanium.

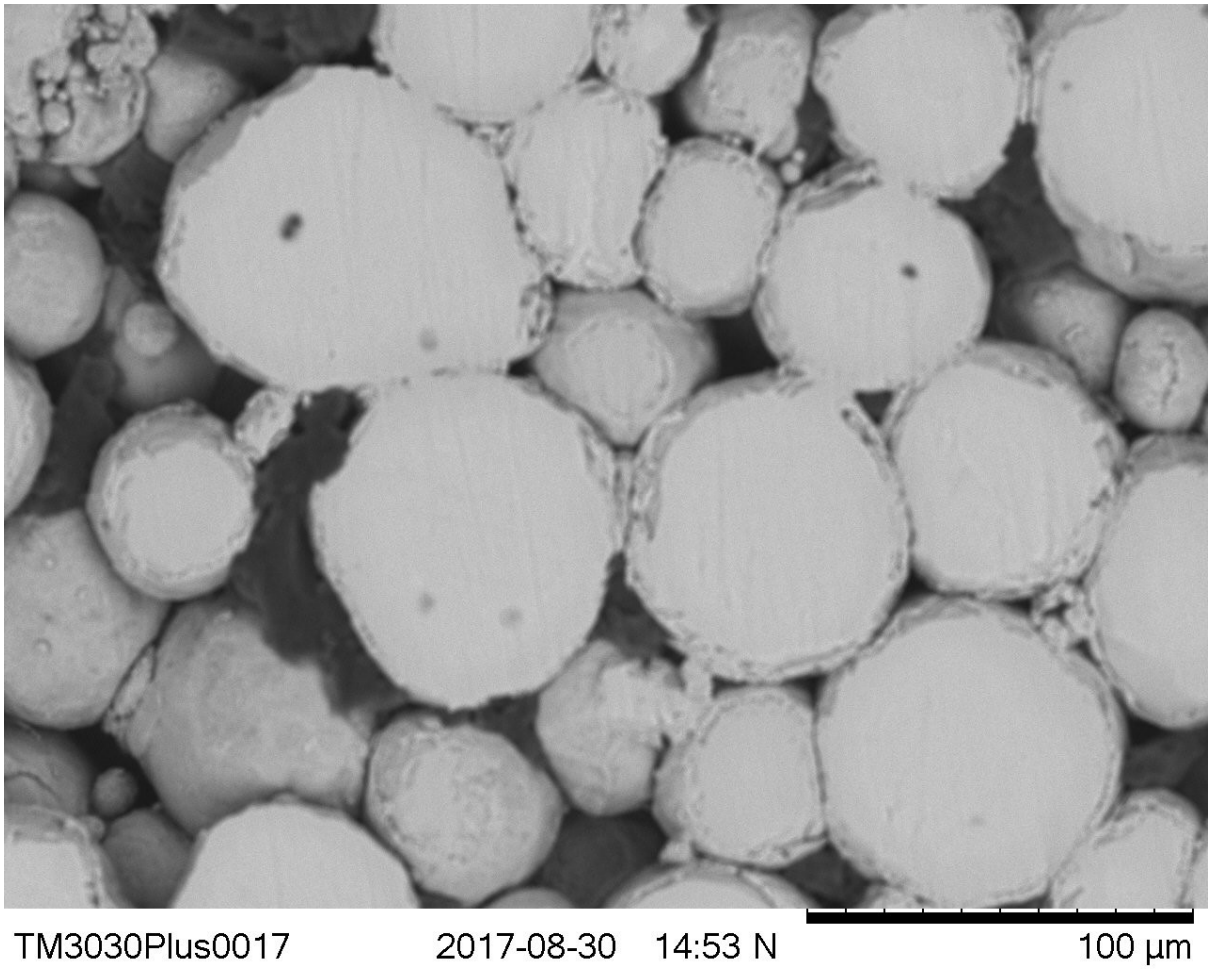

Figure 4.14: SEM backscatter image for nickel plated sample sintered at 1000 ºC for 4 hours showing intermetallic formed along the surface of titanium powder.

4.2 Discussion

From the XRD results, phases formed during sintering of Ti-Ni system were TiNi, $TiNi_3$ and TiO_2. However, only small amount of Ni-Ti powders reacted and formed intermetallics. After intermetallics formed at the interface of adjacent powders, the growth of intermetallics stopped. Intermetallics acted as diffusion barrier and slowed down the diffusion rate of both nickel and titanium atoms. Sintering at different temperatures did not change the phases formed but it changed the amount of phases. SEM and XRD results showed that electroless nickel plating promoted the formation of intermetallics so that the amount of intermetallics formed in electroless plated samples is higher than that of formed in mixed powders. On the other hand, rutile is formed in electroless plated samples.

Using SEM images and ImageJ software pore fractions of samples calculated. While porosity decreased linearly with time in Ni-Cu system, porosity in Ni-Ti system has risen between time intervals 1-2 and then decreased. SEM images showed that time needed for the formation of complete solid solution in Ni-Cu system is between 4-8 hours. However, closure of pores which are close to surface of the pellets takes more time due to unequal stress distribution resulting from pressing of pellets. Electroless nickel plating decreased time needed for complete solid solution.

CHAPTER 5

CONCLUSIONS AND FUTURE WORKS

5.1 Conclusions

This project showed that electroless nickel plating promoted formation of intermetallics in Ni-Ti system. It is obvious from XRD results that amount of intermetallics formed is higher in electroless nickel plated powders. Electroless plated powders formed intermetallics along the powder surface. Electroless nickel plating also increased the diffusion in Ni-Ti system.

Hence, electroless nickel plating can be used for production of shape memory alloys and copper nickel alloys.

5.2 Future Works

Since Ni-Ti alloys mostly used as shape memory alloys and they have equiatomic nickel and titanium composition, composition control of this system is an important issue. Small changes in the composition of shape memory alloys changes the properties of the alloy. Thus, composition of the electroless nickel plated titanium must be more controllable.

Since formation of intermetallics changed in this research, changing the variables such as temperature, heating rate and dwell time may change the formation of these intermetallics. Thus, nickel plated powders should be investigated by changing these variables.

REFERENCES

1. Exner, H. E., “Principles of Single Phase Sintering,” Reviews in Powder Metallurgy and Physical Ceramics, 1, 1-4, 1979, pp. 1-251.
2. Burke, J. E. and J. H. Rosolowski, “Sintering,” General Electric Technical Information Series, General Electric Company, Schenectady, NY, 1973.
3. Pask, J. A., and A. G. Evans ed., University Conference on Ceramics; Ceramic Microstructures ’86: Role of Interface, “Powders, Interfaces, and Processing: Alumina as a Case Study by A. Roosen, S. Sumita and H. K. Bowen,” Plenum, NY, pp. 433-446, 1987.
4. German, R. M., “Sintering Theory and Practice”, John Wiley and Sons, USA, 1989.
5. Coble, R. L., “ Diffusion Models for Hot Pressing with Surface Energy and Pressure Effects as Driving Forces”, J. Appl. Phys., Vol. 41, pp. 4798-807, 1967.
6. Jonghe,L. C., Rahaman, M. N., “Sintering of Ceramics” in S. Somiya Handbook of Advanced Ceramics, Elsevier Inc., 2003.
7. German, R. M. “Sintering Theory and Practice”, 1st Edition, John Wiley & Sons, USA, 1996.
8. Coblenz, W. S., Dynys, J. M., Cannon, R. M., Coble, R. L., “Initial Stage Sintering Models: A Critical Analysis and Assessment”, Sintering Process, Pp. 141-157, New York, 1980.
9. Amar, F., Bernholc, J., Berry, R. S., Jellinek, J., Salamon, P., “The Shapes of First-Stage Sinters”, J. Appl. Phys., 1989, vol. 65, pp. 379-383.
10. Thummler F., Thomma, W., “The Sintering Process”, Met. Rev., vol. 12, pp. 69-108, 1967.
11. Coble, R. L., “ Sintering of Crystalline Solids I. Intermediate and Final State Diffusion Models, J. Appl. Phys., 32, pp. 798-92, 1961.
12. Zhao, J., Harmer, M. P., “Sintering Kinetics at Final Stage Sintering: Model calculation and Map Construction”, Acta Mater., Vol. 52, pp. 4373-78, 2004.
13. Wagner, C., “Theory of Ostwald Ripening”, Z. Electrochem., Vol. 65, pp. 581-91, 1961.

14. Exner, H. E., Petzow, G., and Wellner, P. (1973), ‘Problems in the Extension of Sintering Theories to Real Systems’, in Sintering and Related Phenomena, Kuczynski, G. C., Ed., New York, Plenum Press, pp. 351–62.
15. Rahaman, Mohamed N. “Sintering of Ceramics”, CRC press, 2007.
16. Greskovich, C. "Effect of Green Density on the Initial Sintering of Alumina." Phys.Sintering 4.1 (1972): 33-46.
17. Woolfrey, J. L. "Effect of Green Density on the Initial-Stage Sintering Kinetics of UO2s." Journal of the American Ceramic Society 55.8 (1972): 383-389.
18. C. A. Bruch, Ceramic Bulletin, vol. 41, (12), pp. 799 – 806, 1962.
19. Liniger, E. G., Raj, R., “Sintering of Ordered and Disordered Two-Dimensional Packings” Sci. Sinter., Vol. 21, pp. 109-118, 1989.
20. Yeh, T. S. and Sacks, M. D. (1990), ‘Effect of green microstructure on sintering of alumina’, Ceramic Trans, 7, 309–31.
21. Rhodes, W. W., “Agglomerate and particle size effects on sintering of Yttriastabilized Zirconia”, J Amer Ceram Soc, vol. 64, pp. 19–22, 1981.
22. Qian, M., and G. B. Schaffer. "Sintering of Titanium and Its Alloys." (2010): 324-355.
23. P. W. Lee, Y. Trudel, R. Iacocca, R. M. German, B. L. Ferguson, W. B. Eisen, K. Moyer, D. Madan, and H. Sanderow (eds.), Powder Metallurgy Technologies and Applications, vol. 7 ASM Handbook, ASM International, Materials Park, OH, 1998.
24. A. P. Savitskii, ‘Relation between Shrinkage and Phase Diagram,’ Science of Sintering, 1991, vol. 23, pp. 3–17.
25. Y. Liu and B. R. Patterson, ‘A Stereological Model of the Degree of Grain Boundary-Pore Contact During Sintering,’ Metallurgical Transactions, 1993, vol. 24A, pp. 1497–505.
26. S. Hossein, I. Srinivosan, M. Solveig, “Sintering and Reaction Behaviour in Ni-Ti Powder Mixtures”, Advances in Powder Metallurgy, Vol. 5, pp. 5-45, New Jersey, 2012.
27. Bose, A., Rabin, B. H., German, R. M., “Reactive Sintering of Nickel-Aluminide to Near Full Density”, Powder Met. Intern., vol. 20, no. 3, pp. 25-30, 1988.
28. Wenning, L. A., Lebrat, J. P., Varma, A., “Some Observations on Unstable Self-Propagating High-Temperature Synthesis of Nickel Aluminides” J. Mater. Synth. Process. vol. 2, pp. 125-132, 1994.
29. Sintering, available at hoganas.com, last accessed date: September 2017.

30. A.P. Savitskii, “Liquid Phase Sintering of Systems with Interacting Components”, Russian Academy of Sciences, Tomsk, Russia, 1993.
31. D.A. Porter, K.E. Easterling, Phase Transformations in Metals and Alloys: 2nd Edition, Chapman & Hall USA, New York, NY, (1992).
32. M. Nishida, C.M. Wayman, T. Honma, “Precipitation Processes in Near-EquiatomicTiNi Shape Memory Alloys,” Met. Trans., 17 A, 1505-1515 (1986).
33. Phase diagrams of Binary Nickel Alloys, Ed. P. Nash, ASR international (1991)342
34. N. Bertolino, M. Monagheddu, A. Tacca, P. Giulliani, C. Zanotti, U. A. Tomburini, “Ignition Mechanism in Combustion Synthesis of Ti-Al and Ti-Ni systems” Intermetallics, Vol. 11, pp. 41-49, 2002.
35. ASM Metals Handbook, “Alloy Phase Diagrams”, Vol. 3, ASM International, 1992.
36. www.factsage.com, Last access date: 23.08.2017.
37. Mallory, Glenn O., and Juan B. Hajdu. Electroless plating: fundamentals and applications. William Andrew, 1990.
38. Sviridov V.V., Gaesvskaya T.V., Stepanova L.I., Vorobyova T.N. Electroless Deposition and Electroplating of Metals, Chemical problems of the Development of New Materials and Technologies, Minsk, 2003.
39. A. Brenner and G. Riddel, J. Res. Nat. Bur. Std., 37, 31 (1946); ibid., 39, 385 (1947).
40. Sviridov V. V., Vorobyova T. N., Gaevskaya T. V., Stepanova L. I. Electroless deposition of metals from aqueous solutions. Minsk. 1987. 270 p.
41. D. W. Baudrand, Aircraft Applications for Electroless Nickel Plate, Business Aircraft Meeting, Society of Automotive Engineers, April 1974.
42. P. Ahuja, “Electroless Nickel Coating for Jet Engine Turbine Blades,” Proc. Electroless Nickel Conference, Products Finishing Magazine (1982).
43. Sviridov, V. V., Gaevskaya, T. V., Stepanova, L. I., &Vorobyova, T. N. (2003). Electroless deposition and Electroplating of Metals.
44. Reidel W., “Electroless Nickel Plating”, ASM international, Metals Parks, Oh. (1991), 68-69.
45. Schoenberg, Leonard N. "The use of organic additives to stabilize and enhance the deposition rate of electroless copper plating." Journal of the Electrochemical Society 119.11 (1972): 1491-1493.
46. Fields W., and Zickearff J.R., Electroless, Publication of ASM committee on ENplatting, (1984).
47. Baudrand D. W., Metals Hand book, 8th Edition, (1978).

48. Chow Y., Lau W., and Karim Z., “Surface properties and Solderability Behaviour of Nickel-phosphorus and Nickel-boron Deposited by Electroless Plating “, Surface and Interface Analysis, Vol. 31, (2001), 321-327.
49. F.A. Lowenheim, Modern Electroplating, third edition, John Wiley and Sons, New York, 1974.
50. Rosenberg, Samuel J., “Nickel and Its Alloys”. No. NBS-592. NATIONAL BUREAU OF STANDARDS GAITHERSBURG MD, 1968.
51. Campbell, Flake C., ed., “Elements of Metallurgy and Engineering Alloys”. ASM International, 2008.
52. W. D, Jenkins, T. G. Digges and C. R. Johnson, Tensile properties of copper, nickel, and 70-percent copper-70 percent-nickel and 30-percent-copper 70 percent-nickel alloys at high temperatures, J. Res. NBS 58, 201 (1957).
53. S. J. Rosenberg, “Effect of Low Temperatures on the Properties of Aircraft Metals”, J. Res. NBS 25, 673 (1940)
54. C. L. Guettel, Constantan, Metals Handbook ASM, 8th ed. 1, 1130 (1961).
55. W. F. Roeser and A. I. Dahl, Reference tables for iron-constantan and copper-constantan thermocouples, J. Res. NBS 20, 337 (1938).
56. G. Sorkin, Materials for Submarine Hard Sea Water Systems, J. Naval Engrs. 77, 93 (1965).
57. Duerig, Thomas W., K. N. Melton, and D. Stöckel. Engineering aspects of shape memory alloys. Butterworth-Heinemann, 1990.
58. Kumar, P. K., and D. C. Lagoudas. "Introduction to shape memory alloys." Shape memory alloys (2008): 1-51.
59. Buehler, William J., J. V. Gilfrich, and R. C. Wiley. "Effect of low-temperature phase changes on the mechanical properties of alloys near composition TiNi."Journal of applied physics 34.5 (1963): 1475-1477.
60. Wang, Frederick E., William J. Buehler, and Stanley J. Pickart. "Crystal Structure and a Unique Martensitic Transition of TiNi." Journal of Applied Physics 36.10 (1965): 3232-3239.
61. Novák, P., Pokorný, P., Vojtěch, V., Knaislová, A., Školáková, A., Čapek, J., & Kopeček, J. (2015). Formation of Ni–Ti Intermetallics during Reactive Sintering at 500–650° C. Materials Chemistry and Physics, 155, 113-121.

62. P. Novak, L. Mejzlíkova, A. Michalcova, J. Capek, P. Beran, D. Vojtech, Effect of SHS Conditions on Microstructure of NiTi Shape Memory Alloy, Intermetallics 42 (2013) 85-91.
63. Novák, P., Školáková, A., Pignol, D., Průša, F., Salvetr, P., Kubatík, T. F., & Karlík, M. (2016). Finding the energy source for self-propagating high-temperature synthesis production of NiTi shape memory alloy. Materials Chemistry and Physics, 181, 295-300.
64. Divinski, S. V., Stloukal, I., Kral, L., & Herzig, C. (2009). Diffusion of Titanium and Nickel in B2 NiTi. In Defect and Diffusion Forum (Vol. 289, pp. 377-382). Trans Tech Publications.
65. Gale, W. F., & Totemeier, T. C. (Eds.). (2003). Smithells metals reference book. Butterworth-Heinemann.